FOURIER TRANSFORM
ION CYCLOTRON RESONANCE
SPECTROSCOPY

by

JOE DAVID MELKA

B.S., Michigan Technological University, 1976.

A THESIS SUBMITTED IN PARTIAL FULFILLMENT OF
THE REQUIREMENTS FOR THE DEGREE OF
MASTER OF SCIENCE
IN
THE FACULTY OF GRADUATE STUDIES
THE DEPARTMENT OF CHEMISTRY

We accept this thesis as conforming to the
required standard

THE UNIVERSITY OF BRITISH COLUMBIA

December, 1978.

In presenting this thesis in partial fulfilment of the requirements for an advanced degree at the University of British Columbia, I agree that the Library shall make it freely available for reference and study. I further agree that permission for extensive copying of this thesis for scholarly purposes may be granted by the Head of my Department or by his representatives. It is understood that copying or publication of this thesis for financial gain shall not be allowed without my written permission.

Department of CHEMISTRY

The University of British Columbia
2075 Wesbrook Place
Vancouver, Canada
V6T 1W5

Date DEC. 13, 1978

ABSTRACT

Chapter II of this thesis describes the operation of a Fourier Transform Ion Cyclotron Resonance Spectrometer. Included is a detailed discussion of software which was developed to run the spectrometer and analyze the data. An automatic data acquisition system for kinetic experiments is also described.

Chapter III contains a short discussion of discrete versus continuous methods of data acquisition and problems with the FT-ICR method which utilizes discrete sampling. Two techniques are discussed which have been found to solve problems associated with a digital system, acquisition by "mixing" and zero-filling. Also, mass calibrations done on the FT-ICR spectrometer are presented.

The reactions of some negative ions with esters in the gas phase have been studied by FT-ICR and are discussed in Chapter IV. The reactions of ^{18}O labelled methoxide with methyl trifluoroacetate, methyl benzoate, dimethyl carbonate, diethyl carbonate and dipropyl carbonate have been studied. It was found that there is incorporation of ^{18}O in product ions of the form $RCOO^-$ showing that methoxide attacks esters in the gas phase partially at carbonyl carbon. Product distributions are found to be consistent with two competing mechanisms, $B_{AC}2$ and S_N2. Thus it was found that $CH_3{}^*O^-$ reacts with $C_6H_5COOCH_3$ 92% by a $B_{AC}2$ type mechanism and 8% by an S_N2 type mechanism. The amount of ^{18}O incorporation in

product ions was seen to decrease with the presence of β hydrogens due to the presence of an elimination channel. The reaction of ethoxide with the above named esters was studied and the products are also interpreted in terms of three competing mechanisms, $B_{AC}2$, S_N2 and elimination.

TABLE OF CONTENTS

LIST OF FIGURES

LIST OF TABLES

ACKNOWLEDGEMENTS

I would like to acknowledge the support and encouragement of Professor Melvin Comisarow during my career at U.B.C.. Also, thanks must be extended to the technical staff at U.B.C. who provided much needed advice and service.

At this time it gives me great pleasure to cite the efforts of my colleagues and good friends, Dr. Gérald Parisod and Valerio Grassi. Without their co-operation and assistance, this thesis would not have been possible.

Thanks must also be provided to the following people for various services performed: Barry Hames (proofreading), Howard Morton (G.L.C. analysis), Gord Rickards (advice on synthesis) and Randy Mikula (worthy basketball opponent).

Last but not least, I would like to thank my parents for supporting my educational goals and offering needed encouragement.

"I don't get no respect."

Rodney Dangerfield,
famous comedian.

I. INTRODUCTION

Reactions between ions and neutral molecules in the gas phase have been actively studied by many experimental techniques during the past two decades. Various types of instrumentation which have been developed to perform these studies include tandem-mass spectrometers, drift tubes, high pressure mass spectrometers and ion cyclotron resonance (ICR) spectrometers.[1,2] The studies of ion-molecule reactions can be divided into two broad areas, thermodynamics and kinetics.

Thermochemical properties that have been studied include proton affinities, electron affinities, acidities, basicities, ionic heats of formation and Lewis acid-Lewis base interactions. These results have been obtained by measurements in the absence of a solvent so that the intrinsic properties of a molecule are revealed. Gas phase results can be compared to solution results to provide interesting contrasts and comparisons. Exemplifying the differences between solution and gas phase reactions is the following gas phase basicity order which was discovered by Brauman and Blair[3]

$$MeO^- > EtO^- > t\text{-}BuO^-$$

This is in contrast to the well known solution order

$$t\text{-}BuO^- > EtO^- > MeO^-$$

The difference has been explained by polarizability effects which determine the gas phase basicity order as compared to in solution where solvent effects dominate. By studying

families of compounds in the gas phase and comparing to solution results, much can be learned about solvation effects which leads to a better understanding of chemical reactions.

On the kinetic front, theories have been advanced to describe factors which influence collision rates and reaction rates. Notable developments in the past decade include the average dipole orientation (ADO) theory which is used to describe the collision frequency between an ion and a polar molecule.[4] And, the theory of unimolecular decomposition has successfully been used to describe the fragmentation to products of a reaction intermediate for some S_N2 reactions in the gas phase.[5] The sum of thermochemical and kinetic information obtained from gas phase studies can then lead to a better understanding of the forces which control a chemical reaction.

ICR is a powerful tool for determining absolute and relative rate constants, making equilibrium measurements to establish acidity and basicity scales, probing reaction mechanisms, determining electron affinities by photodetachment experiments and elucidating complex reaction schemes by double resonance techniques.[2] This thesis describes work which applies the technique of Fourier transform ion cyclotron resonance (FT-ICR) spectroscopy to the study of negative ions with esters in the gas phase. FT-ICR is a new method for studying gas phase reactions which has recently been developed and has been shown to have advantages in resolution, speed, mass range and sensitivity over conventional ICR methods.[6]

Chapter II of this thesis describes the FT-ICR spectrometer used for this work and how it operates. Included is a detailed discussion of software which was developed to run the spectrometer and analyze the data. An automatic data acquisition system for kinetic experiments is also described.

Chapter III contains a short discussion of discrete versus continuous methods of data acquisition and problems with the FT-ICR method which utilizes discrete sampling. Various techniques are presented for solving problems associated with a digital system. Examples are presented which show typical experimental problems in FT-ICR and how they are solved. Also, the problem of mass calibration is discussed and the results of mass calibrations done on an FT-ICR spectrometer are compared favorably with calibrations done on a conventional instrument.

Chapter IV discusses the reactions of some negative ions with esters in the gas phase as studied by FT-ICR. The reactions of methoxide and ethoxide with methyl benzoate, methyl trifluoroacetate and three alkyl carbonates (methyl, ethyl and n-propyl) have been investigated. Extensive labelling schemes have been used to probe mechanistic pathways. It is shown that for the esters used in this study, numerous pathways exist that lead to products. Rates have been determined using the data acquisition system presented in chapter II and compared to ADO theory to obtain reaction efficiencies. Various mechanistic possibilities are discussed and the reactions of carbonates are compared to the

the reactions of other esters with negative ions in the gas phase.

REFERENCES

1. P. Ausloos (Ed.), "Interactions Between Ions and Molecules", Plenum Press, New York, 1975.

2. T. A. Lehman and M. M. Bursey, "Ion Cyclotron Resonance Spectrometry", John Wiley and Sons, New York, 1976.

3. J. I. Brauman and L. K. Blair, J. Am. Chem. Soc. 90, 6561(1968).

4. Reference 1, pages 163-183.

5. W. N. Olmstead and J. I. Brauman, J. Am. Chem. Soc. 99, 4219(1977).

6. M. Comisarow in "Advances in Mass Spectrometry", N. R. Daly (Ed.), Heyden and Son Ltd., London 1978.

II. THE FT-ICR SPECTROMETER

A. Introduction to ICR Theory

Ion Cyclotron Resonance Spectroscopy is a form of mass spectroscopy that is particularly suited for the study of ion-molecule reactions. Numerous review articles describe in detail the theory of ICR and the types of experiments that can be done by this method.[1-3] Consequently, only a brief introduction to the technique will be given here.

A typical ICR experiment is conducted by forming ions in an ion trap, called a cell, which is enclosed in a vacuum chamber containing appropriate sample gases at pressures of 10^{-9} to 10^{-4} Torr. After a suitable delay time which ranges from milliseconds to seconds, the ions in the cell are detected. By varying the time between formation and detection of the ions, the reactions of ions with a neutral gas can be followed. Trapping voltages are used to keep ions of a certain sign in the cell. Reversing the polarity of the trapping voltage effectively removes the ions from the cell, a process commonly referred to as a quench pulse. A general pulse sequence is given in figure 1 which illustrates the pulsed ICR technique; formation of ions, reaction time, detection and quench.

It is well known that an ion of charge q and mass m in a homogeneous magnetic field of strength B will be constrained to a circular path that is perpendicular to the magnetic field and will orbit at a cyclotron frequency ω where

$$\omega = qB/m \qquad (2\text{-}1)$$

A mass spectrum is obtained by determining the frequencies of the sample ions and then converting to masses by equation 2-1.

Conventional ICR spectrometers detect ions in the following manner. A radiofrequency electric field is used to excite the motion of the sample ions by connecting the output of the RF oscillator to the top and bottom plates of the ICR cell (see figure 4). If the frequency of an ion is equal to the frequency of the applied RF field, the ion will absorb energy from that field, a process called ion cyclotron resonance. A marginal oscillator circuit provides the RF field as well as measuring ion intensities by relating power absorbtion from the circuit to the number of ions which are in resonance. By varying the magnetic field, the sample ions are equated with the fixed frequency of the marginal oscillator circuit and detected. A plot of power absorbtion of the circuit versus magnetic field strength leads to a mass spectrum. This method of detection, although proved to be very reliable, has several drawbacks. Since only one frequency can be detected at a given time, it can take up to 20 minutes to record a mass spectrum of m/e = 15 to 200. Also, resolution is poor.

An alternate method of detection involves exciting the cyclotron motion of all the ions in the cell and detecting the voltage induced in the top and bottom plates of the ICR cell after the RF field is removed.[4] The signal will oscillate with time due to the cycloidal motion of the ions. In this

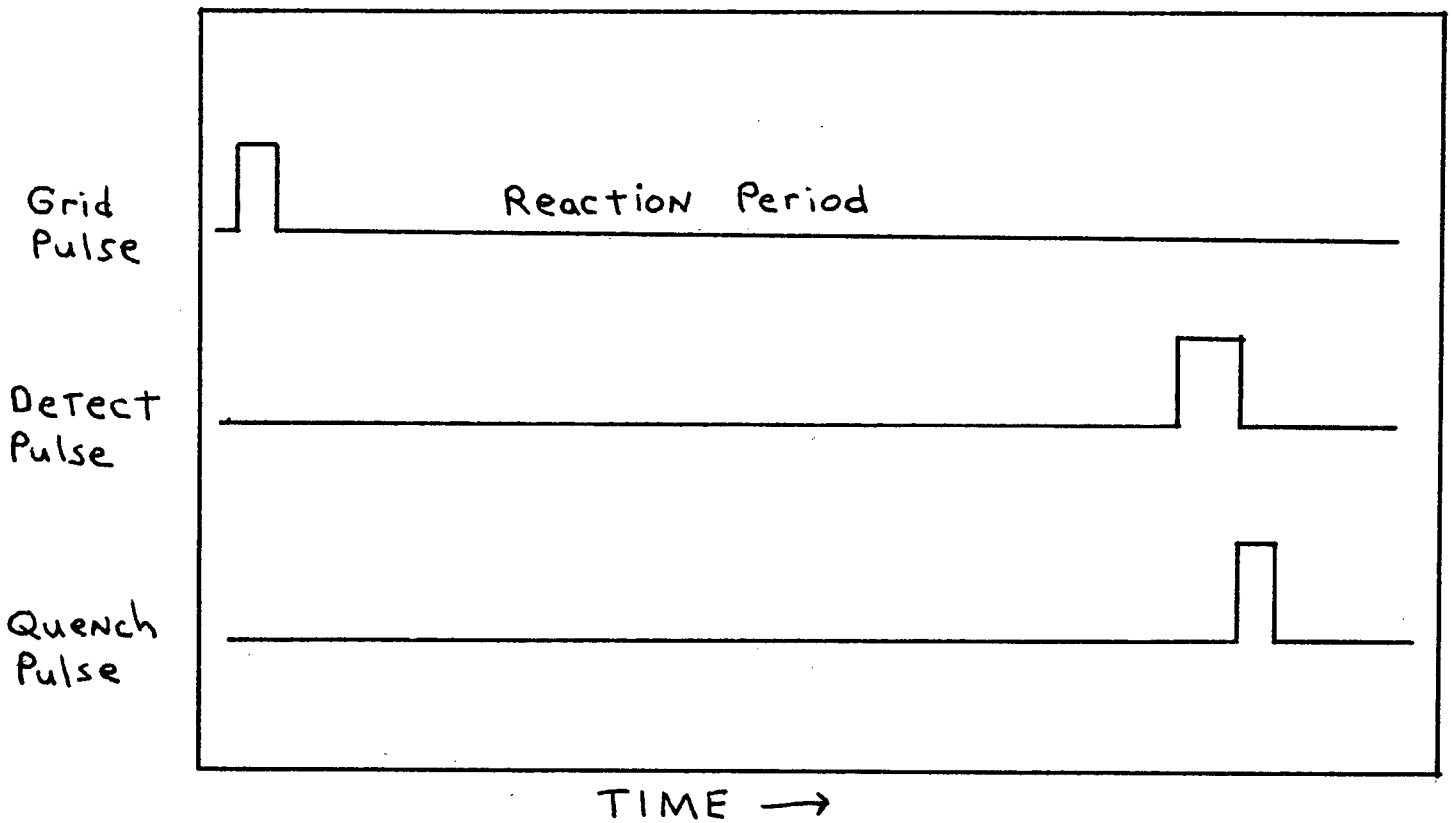

Figure 1 General ICR pulse sequence.

method, excitation and detection are temporally distinct. The time domain signal can be Fourier transformed to give the corresponding frequency domain spectrum. A large saving in time is realized as all the frequencies are detected in the same time it takes to detect one frequency by the conventional method. Sensitivity is enhanced through the use of signal averaging and the useful mass range has been extended to at least 1200.

B. The FT-ICR Spectrometer

i. Overview

The FT-ICR spectrometer used in this work was built in the chemistry department at the University of British Columbia. The remainder of this chapter will be devoted to describing the instrument and software that runs the spectrometer and processes the data in detail. The main parts of the FT-ICR spectrometer are the vacuum system, cell, magnet and computer with its associated programmable pulser and RF generator.

ii. Vacuum System

A diagram of the vacuum system is given in figure 2. The vacuum container is made of stainless steel and is designed such that the end containing the ICR cell will fit between the poles of a 24 kGauss magnet. The magnet is on a track, making it moveable, thus facilitating repairs to the vacuum system and bake-out. The main vacuum system is pumped by a 225 l/s Veeco MagIon pump which can be valved off by a bellows valve. Base pressures of the system after overnight bake-out are typically 2-4 x 10^{-10} Torr as measured with a Varian

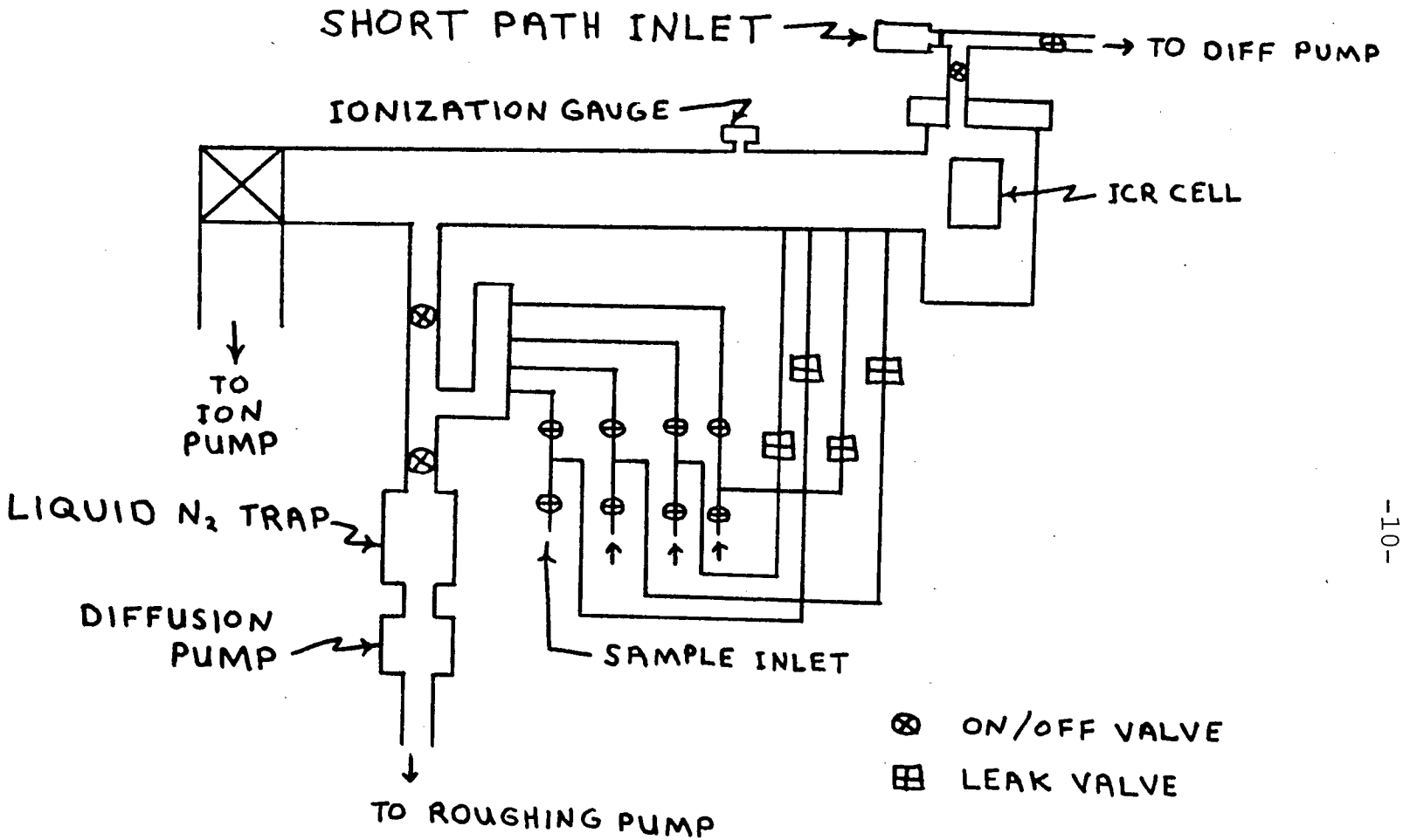

Figure 2 Schematic diagram of the FT-ICR vacuum system.

Model 971-1008 ionization gauge. The ionization gauge can be calibrated for various gases in the range 10^{-5} to 10^{-4} Torr by a Baratron capacitance manometer. It is assumed that the Baratron gives the true pressure in this pressure range. However, ICR experiments are usually conducted at lower pressures neccessitating calibration of the ion gauge against the Baratron at these higher pressures. Figure 3 shows a calibration curve for CH_4. A calibration factor $P_{Baratron}/P_{Ion\ Gauge}$ can be determined from the slope of the line. The pressure is then equal to the ion gauge reading multiplied by the calibration factor which is assumed to be constant over a wide pressure range.

Sample introduction can be accomplished by two methods, leaking vapors into the vacuum system or by using a short path inlet for nonvolatile liquids and solids. Four inlets, equipped with ₸14 male adapters welded to Cajon fittings are available for sample introduction. Sample gases are leaked into the main vacuum system by adjustable leak valves. The inlet system is pumped by an 11 l/s diffusion pump which is separated from the sample containers by a liquid nitrogen trap. A mechanical pump is used as a forepump. Involatile samples can be introduced by placing them in a glass tube which has been sealed to a Cajon fitting. A simple on/off valve separates this short path inlet from the main vacuum chamber. Dynamic pressure regulation is accomplished by manipulation of the bellows valve. The short path inlet can also be pumped by the diffusion pump.

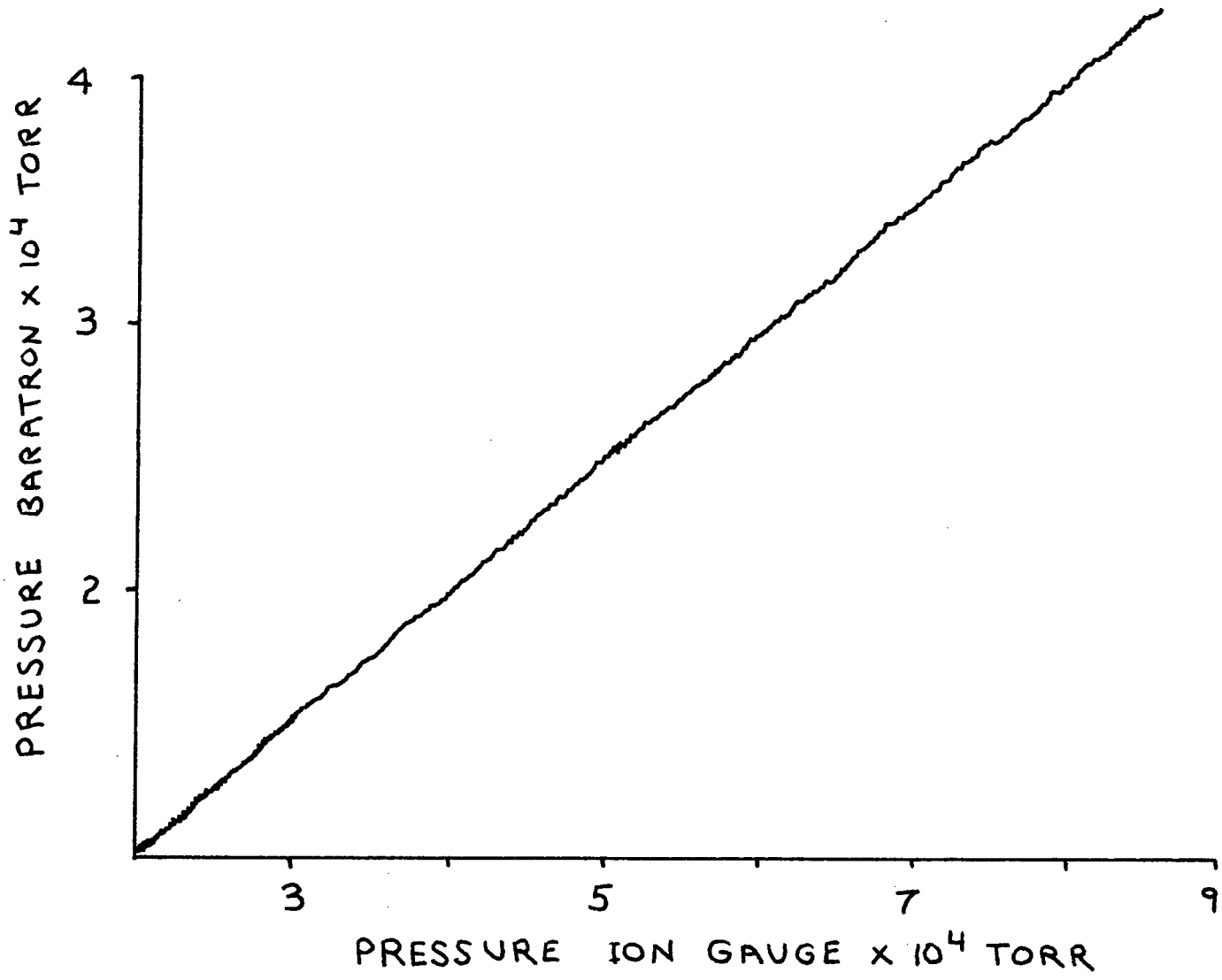

Figure 3 A sample Baratron pressure v. Ion gauge pressure plot for CH_4.

The entire vacuum system, except the part containing the cell, called the can, and the ion pump is housed in a large box which is lined with insulation and equipped with heaters for bake out purposes. The ion pump can be heated by four tubular heaters which extend into the ion pump body and a removeable can heater was built to heat the cell area. Bake out temperatures reach 180°C in the can area and 120 °C in the main system. After the main vacuum system has been opened to the atmosphere, it can be pumped down by the diffusion pump to a pressure of about 10^{-6} Torr. At this point, the ion pump can be started and the diffusion pump valved off. It was found that with no liquid nitrogen trap, backstreaming of diffusion pump oil vapors into the main system during pump down was a problem, identified by burping, i.e., sudden pressure fluctuations in the ion pump at lower pressures. Addition of the trap solved this problem.

iii. ICR Cell and Signal Route

A cubic trapped ion cell similar to the original McIver design is used.[5] The cell is illustrated in figure 4. Trapping voltages are applied to plates T to trap ions in the magnetic field. It is also possible to apply suitable voltages to plates N, S, E, W for tuning purposes. A grid of copper mesh is placed between the trapping plate and the rhenium filament. By biasing the grid potential, electrons can be pulsed into the cell at the appropriate time and their current measured by a collector on the opposite trapping plate.

RF excitation is applied to plates E and W. The signal

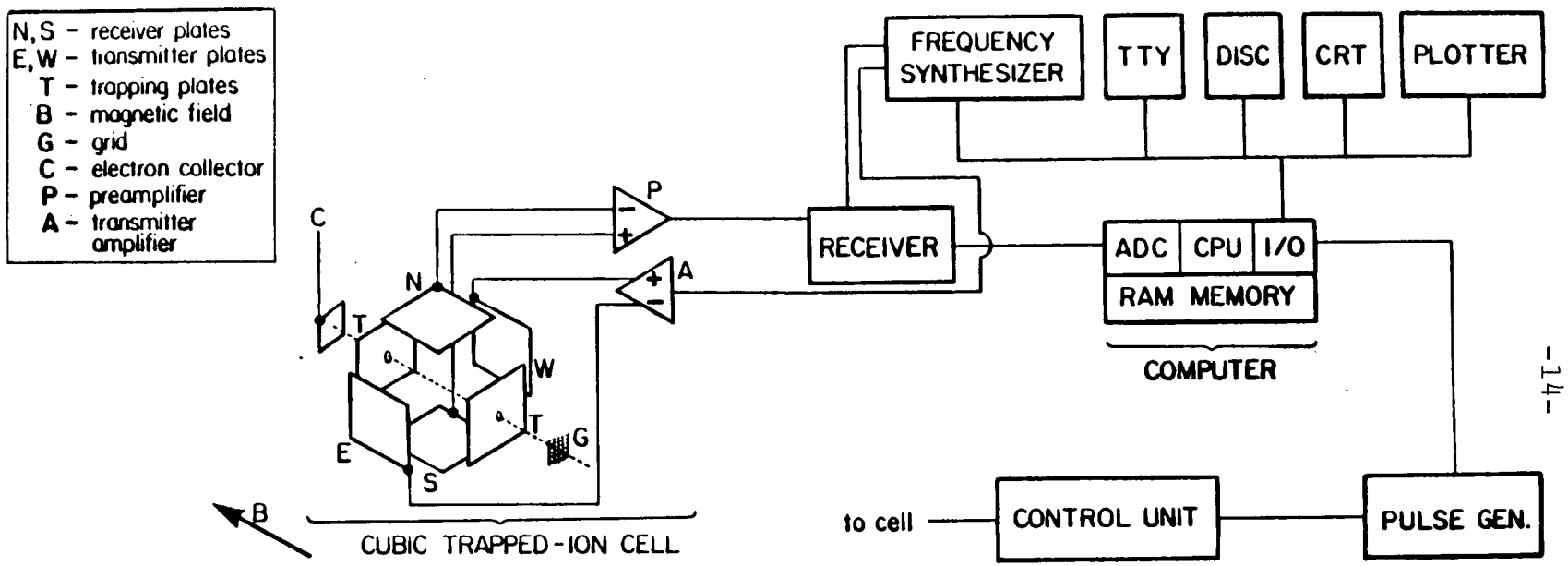

Figure 4 Schematic diagram of the FT-ICR spectrometer.

induced in plates N and S by the excited ion motion is amplified by a 60 dB preamp, subjected to a high pass filter and amplified again by 20 dB. The signal can now be fed directly into the computer's analog-digital converter (ADC) and subjected to Fourier transformation. This process is known as "direct acquisition" and is illustrated in figure 5. Alternately, the signal can be mixed with a reference frequency, passed through a low pass filter to extract a certain band of frequencies and then digitized. This is known as "mixing" and is illustrated in figure 6.

iv. Computer, Pulser, Disk and Synthesizer

The spectrometer is controlled by a Nicolet 1180 minicomputer which has 24k memory and uses 20 bit words.[6] Either assembly language or BASIC can be used for programming. The computer is equipped with a fast ADC which operates in various manners depending on the digitization rate. For signals up to 333 kHz, the ADC has 12 bit resolution and the digitized signal is fed directly into the randon access memory (RAM). For signals from 333 kHz to 2.5 MHz, the ADC still has 12 bit resolution but the digitized signal can't be fed directly into the RAM at this high rate so the signal is fed into a buffer memory, or shift register memory, and then at a slower rate fed into the RAM. For signals from 2.5 to 5 MHz, 9 bit resolution is obtained and the buffer mode is used. Programs and spectra can be stored on a magnetic disk which has room for 1,143,296 words of 20 bits each or about 60 spectra of 16k words each.

RECEIVER CONFIGURATION FOR DIRECT ACQUISITION

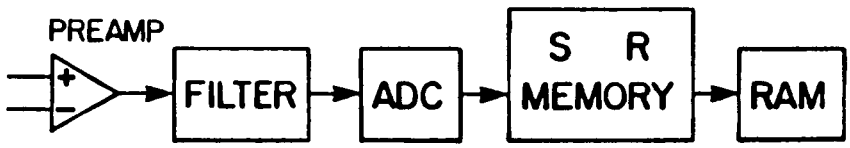

Figure 5 Receiver configuration for direct acquisition

RECEIVER CONFIGURATION FOR SPECTRAL SEGMENT EXTRACTION

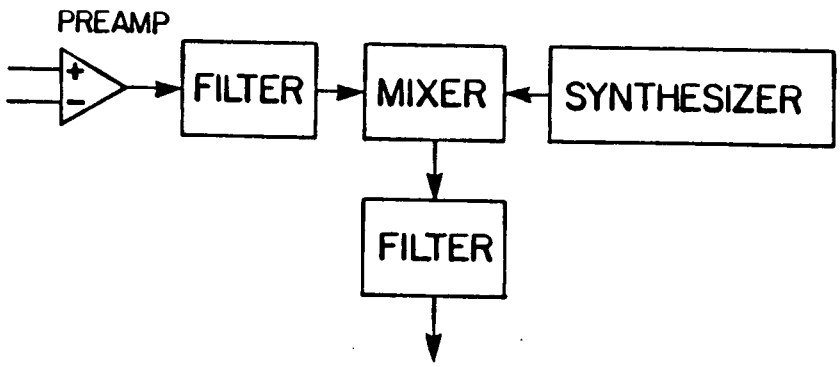

Figure 6 Receiver configuration for spectral segment extraction or mixing.

A Nicolet 293-A programmable pulser which has 16 memories and 7 output lines is used to send pulses to appropriate devices in the spectrometer thereby controlling the experiment. The 293-A is under control of the computer so that pulse lengths can be easily altered as well as the pulse sequence changed to suit the experiment. Pulse lengths range from 32 ns to 2147 s. Pulses from the 293-A can be used to turn devices on and off. Also, an interrupt pulse can be sent to the computer which will then determine what the value of the 293-A program counter is.

Different program counter numbers are associated with different subroutines that will be executed by the computer when it receives an interrupt pulse. This is how the frequency synthesizer outputs at the correct time during the pulse sequence a double resonance ejection frequency, an excitation frequency band and a mixing frequency. A frequency sweep excitation is used to excite the cyclotron motion of the ions. A desired frequency band is covered in steps of .875 μs, each step being a certain frequency jump. Thus to excite a band of 200 kHz using a step size of 200 Hz will take .875 ms.

Since the frequency synthesizer generates up to three different outputs on the same line during each pulse sequence, switching circuitry was built to route the output to the appropriate place.[7] The switching circuitry is activated by pulses from the 293-A.

v. Electron Ejection

When dealing with negative ions, it is common to trap stray electrons in the cell. If negative ions can be formed by the dissociative attachment of thermal electrons to neutral molecules, i.e., $CH_3ONO + e^- \longrightarrow CH_3O^- + NO^\cdot$, the total ion concentration will not be constant as a function of time if electrons are trapped in the cell. The frequency of an electron is much too high for conventional double resonance techniques; that is, application of an RF pulse to plates E and W at the frequency of an ion to be ejected.

Beauchamp has shown that an ion in an electric (trapping) field will have a certain oscillatory frequency in the trapping field.[8] This fact can be used to eject electrons by applying an RF pulse to the trapping plates. A Wavetek signal generator capable of generating signals up to 30 MHz was used to eject electrons. A simple delay circuit was used to send this pulse to the cell a certain time after the beam pulse had been completed to eject any stray electrons. This technique yields total ion intensities that are constant with time if the emission current is high. Total ion intensities that are constant with time can also be obtained if a low emmision current and no electron ejection are used.

C. Software

i. FTZB and the Pulse Sequence

FT-ICR experiments are under control of a program called FTZB. This program was written in assembly language and is approximately 8 k words in length leaving 16k of

memory for data acquisition and display purposes. FTZB is an extremely powerful tool for running double resonance experiments and collecting data for kinetic experiments. This program will be explained in detail as a thorough knowledge of its workings manifests itself in a rigorous understanding of how an FT-ICR experiment is performed.

The pulse sequence for FTZB is given in figure 7 where PC refers to the program counter number in the 293-A which starts at zero.[9] The pulse sequence in figure 7 is essentially the same as the pulse sequence in figure 1 with the exception that detection is performed in a different manner and pulses for double resonance ejection experiments have been added.

Various parameters critical to the experiment such as starting frequency of the excitation sweep, width of the excitation sweep, digitization rate, reaction time, mixing frequency and beam length are either typed into the computer or set using control knobs on the front of the computer. The pulse sequence is initiated by a subroutine called GO. The computer will load the 293-A programmable pulser with timing words which tell the 293-A how many pulses are to be outputted on each of its seven output lines during the pulse sequence and the duration of each pulse. Table 1 lists the output pulses and their uses. The pulse sequence is given in figure 7.

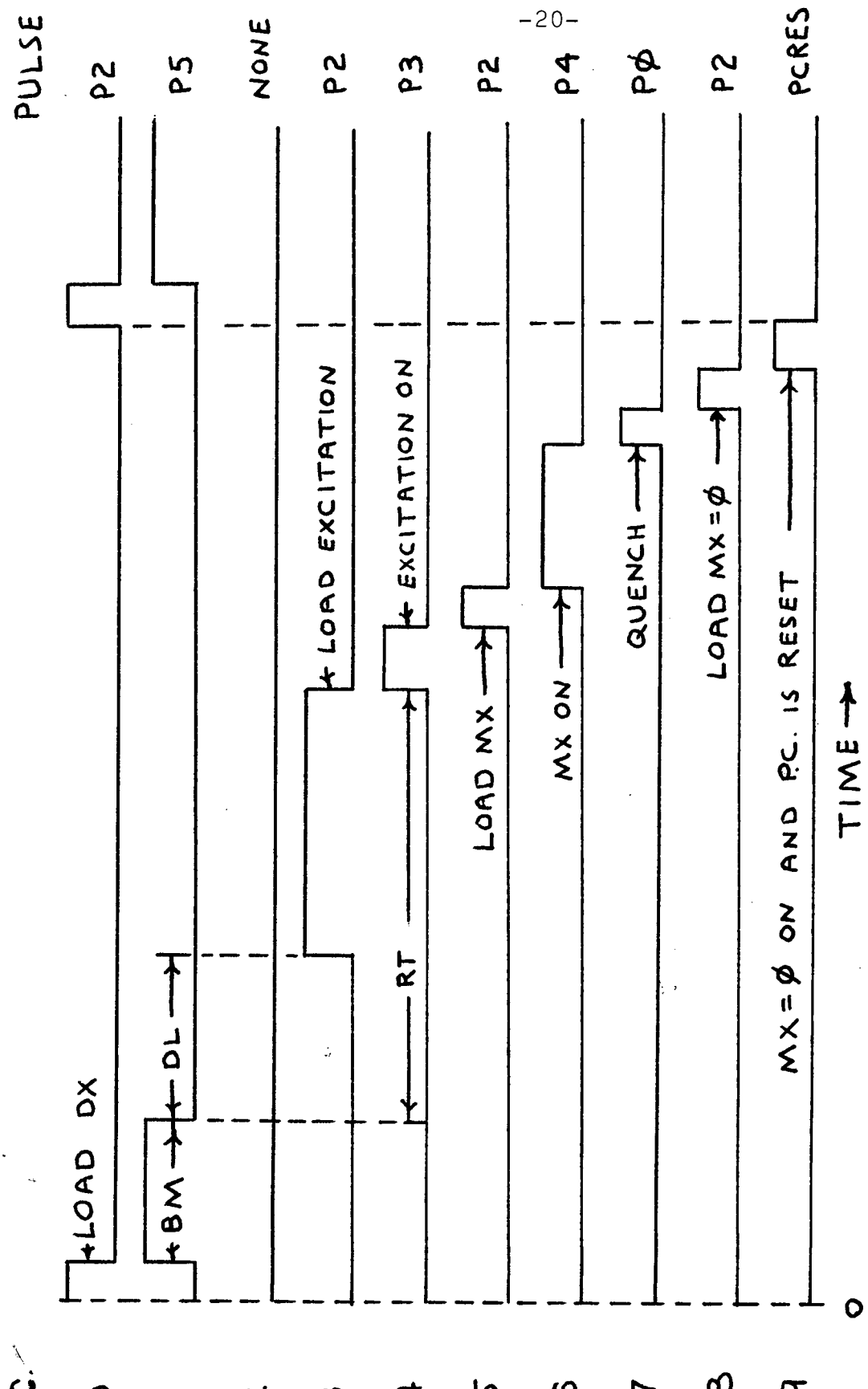

Figure 7 Pulse sequence for FTZB.

Table 1 Output Pulses From 293-A and Their Uses

Pulse Number	Use
P0	Quench
P2	Interrupt
P3	Transmitters On
P4	Receiver On
P5	Beam
P6 or PCRES	Reset PC

The first output of the 293-A is sent back to the computer, a process called an interrupt. Receiving an interrupt tells the computer to search its list of subroutines to find the appropriate one to execute when the PC is at a certain number. When the PC is 1 (after a pulse is initiated, the PC is incremented by one so that even though the zero pulse is still on, the PC has a value of 1), the computer executes a subroutine that loads the Rockland frequency synthesizer with the double resonance frequency if a double resonance experiment is being done, otherwise a frequency of zero is loaded. The loading process takes .3 ms.

After .3 ms, the output on line P2 goes from a high to a low value signalling the Rockland frequency synthesizer to begin output of the double resonance frequency which is sent to the cell. Simultaneously, the beam pulse (P5) which biases the grid to allow electrons into the cell, forming ions, is turned on. At this point, ions are being formed in the cell and ions of a certain frequency are being ejected if a double resonance experiment is being done.

After the beam pulse, there is a delay of length DL

which means length of double resonance pulse after beam. No output from the 293-A is used here, it just acts as a timer. After time DL, an interrupt pulse (P2) is again sent to the computer which executes a subroutine which loads the Rockland controller with frequency sweep excitation parameters. This interrupt pulse effectively ends the double resonance ejection period as new parameters are loaded into the Rockland. Pulse P2 is kept on until time RT from the end of beam has passed. Loading the Rockland controller only takes a fraction of a millisecond but in some experiments it is desirable to have a longer time between the end of double resonance ejection and detection.

Frequency sweep excitation begins when P2 is turned off and P3 is turned on. P3 activates switching circuitry that sends the frequency sweep excitation to plates E and W. So far, ions have been formed, some ejected, allowed to react for time RT and their cyclotron motion excited by frequency sweep excitation.

When the excitation is complete, an interrupt (P2) is again sent to the computer from the 293-A telling the computer to load the mixing frequency MX, into the Rockland if acquisition is to be done via the mix mode as in figure 6.

When P2 goes down, the Rockland begins to output the mixing frequency and simultaneously pulse P4 is sent to the computer's ADC instructing it to begin digitization of the ICR signal. The ICR signal has been taken from plates N and S, amplified, filtered and sent to the ADC directly or

mixed with a reference frequency to extract a band of frequencies and shift them to lower values, thereby allowing for slower digitization rates. Output from the Rockland always starts at the same phase value, therefore the digitized ICR signal can be coherently added from scan to scan to increase sensitivity.

Acquisition time is dictated by digitization rate and the number of data points to be collected. When acquisition is complete, P0 (quench) reverses the sign of the trapping field, thereby ejecting any ions remaining in the cell, a process called quench. Another interrupt (P2) is sent to the computer after the quench pulse, telling the computer to load a frequency of zero into the Rockland, ending the mixing frequency output. The last pulse, P6, is sent to the computer instructing it to set PC to zero.

The pulse sequence is repeated over and over until the desired number of scans, NS, has been completed. After each scan, the digitized ICR signal is added to the values in memory. This is known as signal averaging. If noise in the system is random, signal to noise enhancement is $(NS)^{\frac{1}{2}}$ where NS is the number of scans. The digitized transient ICR signal now resides in memory where it is amenable to Fourier transformation, storage on disk or other treatment.

ii. Double Resonance

Ft-ICR double resonance experiments have recently been discussed elsewhere so only a cursory mention will be made here.[10,11] FTZB was written such that an ion can be ejected

for any period of time up to excitation, allowing .3 ms for loading of the excitation parameters into the Rockland controller. Hence FTZB is very versatile and as such it is a powerful tool for elucidating ion molecule reaction pathways via double resonance experiments.

iii. Kinetic Data Acquisition By FTZB

One of the useful features of ICR is the ability to determine rate constants for ion molecule reactions. FTZB was written for the acquisition of spectra at various reaction times and the storage of said spectra on disk for analysis to determine rate constants. Since the density of ions is orders of magnitude smaller than the neutral gas density at ICR pressures, it is assumed that the disappearance of an ion is a pseudo first order process,

$$A^- + B \xrightarrow{k} C^- + D \qquad (2\text{-}2)$$

The concentration of A^- is simply

$$[A^-] = [A^-]_{t=0} e^{-k't} \qquad (2\text{-}3)$$

where k' is the rate of disappearance of A^- and t is time. k' is converted to an absolute rate constant by dividing k' by the neutral gas density.

Various options were written into FTZB for the kinetic experiments. The first reaction time is typed into the computer along with the reaction time increment, that is how much the reaction time changes between each spectrum. Also, the number of files (spectra) to acquire and the name of the first file is entered. A double resonance option allows the length of the double resonance pulse (DL) to be incremented

between spectra by the reaction time increment or kept constant. Thus, continuous ejection of an ion is possible even though the reaction time is changing. The file names are in the format FILE01.EXT where FILE and EXT are chosen to be descriptive of the experiment and 01 is the number of the first file. File numbers can range from 01 to 99.

The first ICR transient is collected at the initial reaction time and automatically stored on disk with the name FILE01.EXT. The reaction time is then incremented, also DL if desired, and a second ICR transient signal collected and stored on disk with the name FILE02.EXT. This process continues until the desired number of files is stored on disk.

Three options, chosen at the start of the experiment, are available for treatment of the transients on the disk. 1) Leave the transients on disk as is for future analysis. 2) Automatically call the transients off the disk and Fourier transform them, then store the transformed spectra back on the disk with the file name FILEXY.EXT where XY is a running number that begins with a value that is one more than the number of the last acquired ICR transient. 3) Do the same as option 2 except that the Fourier transformation is over a longer data set than the original data set. This is known as zero-filling and is discussed in more detail in Chapter 3. The maximum transformation by FTZB is 16K points. No intervention by the operator is needed after the initial parameters and options have been selected and the start command, JO, has been given. Thus acquisition of kinetic data is

automatic and fast.

iv. Peak Picking

ICR frequency domain spectra contain peaks which must be identified by frequency (or mass) and intensity. A program called CUBS was written in BASIC to do just this.

Briefly, CUBS operates in the following manner. The operator types in the file name, starting frequency of the file, spectral width and number of points in the file. The program then calls the file off the disk and calculates the mean noise for the spectrum and finds the largest peak simply by looking for the maximum point in the spectrum. Both the mean noise and the maximum are printed out. The operator then chooses a value for the threshold of a peak and types it into the computer. Usually the threshold is at least five times the value of the mean noise. CUBS then searches for peaks using an algorithm published by Cooper and after the search is completed, outputs the frequency of each peak, intensity and relative intensity.[12] Relative intensity is determined by comparing each peak to the largest peak which is assigned a value of 100.

Fourier transformation of an ICR time domain signal will result in a frequency domain spectrum. That is, the spectrum is linear in frequency not mass. CUBS has an option for converting frequencies into masses and for plotting a spectrum linearly in mass. The accuracy of conversion of frequencies into masses is discussed in Chapter 3. It will be seen that mass calibrations done by FT-ICR are better than mass calibrations done by conventional ICR.

v. Rate Determinations

Peak picking of spectra with many points is very time consuming. Therefore, a second program called PIK was written in BASIC to get the peak intensities in many spectra; but the frequencies of the peaks must be known before using this program. PIK simply calls a spectrum off the disk, goes to the first frequency that was entered by the operator and prints out the intensity at that frequency. It then goes to the next frequency that was input and prints out the intensity at that frequency, etc.. Output for each file is frequency, intensity and relative intensity. PIK does this for the desired number of files.

Also included in PIK is an option for kinetic analysis. A frequency is selected, pressure of the neutral gas entered and the calibration coefficient for the ionization gauge is also typed into the computer. PIK then determines the intensity of the peak at that frequency from each spectrum that was recorded at different reaction times by FTZB. From a least squares analysis, a slope of the decay of that ion with time is determined along with a correlation coefficient. The slope is converted to an absolute rate constant by dividing by the number density of neutral molecules. Rates are printed out in units of cm^3/molecule-sec. Using the combination of FTZB and PIK, rate determinations are fairly fast.

The standard reaction for rate determinations in the field of ion molecule reactions is

$$CH_4^+ + CH_4 \longrightarrow CH_5^+ + \cdot CH_3 \qquad (2\text{-}4)$$

An average rate of 1.11×10^{-9} cm^3/molecule-sec has been obtained for this reaction using various experimental techniques.[13] Figure 8 shows some CH_4 data which was obtained by using FTZB and PIK. Using the calibration from figure 3, the rate of decay of CH_4^+ was found to be $1.11 \pm .02 \times 10^{-9}$ cm^3/molecule-sec, in good agreement with the literature value.

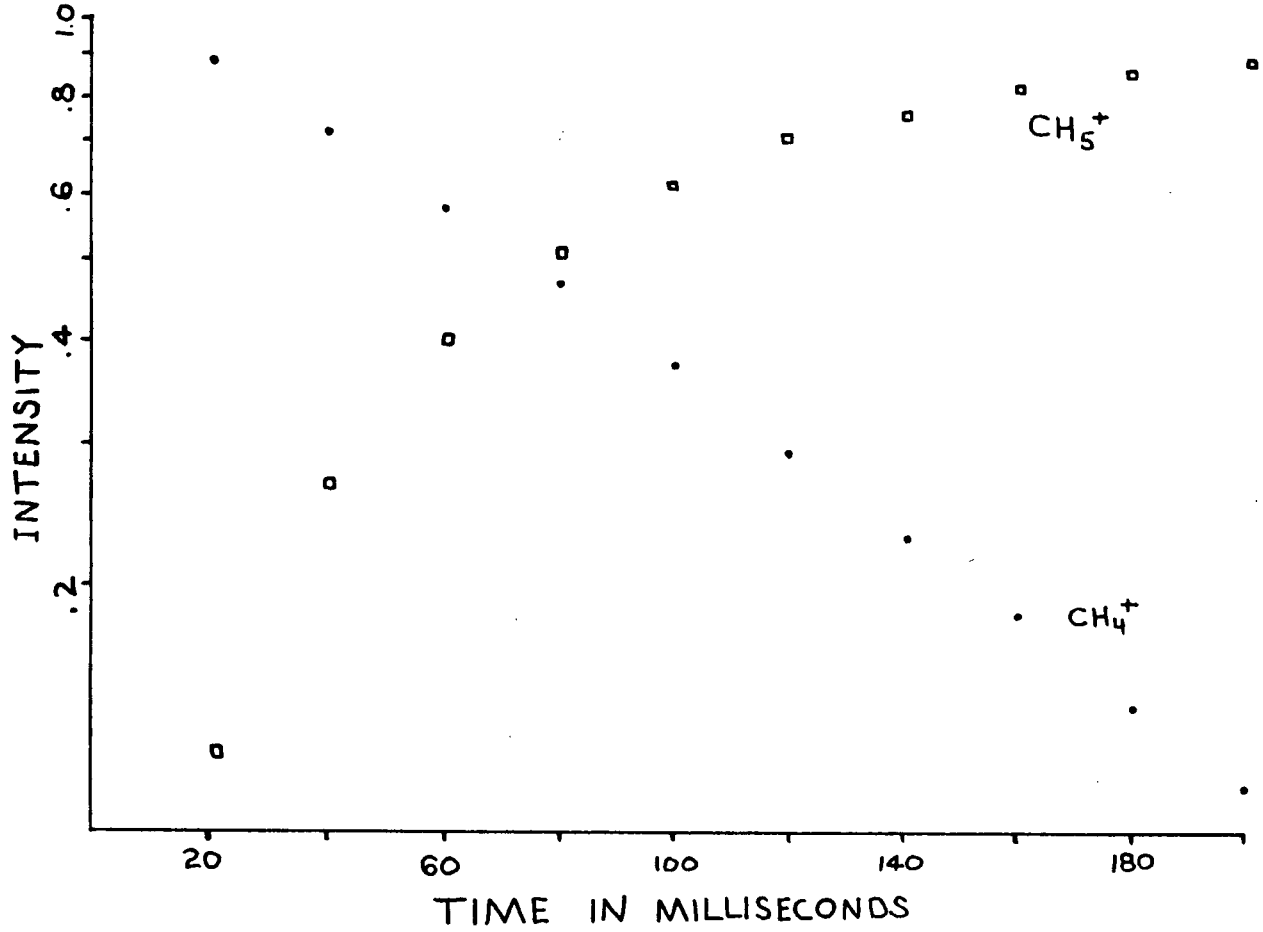

Figure 8 Time plot for the reaction $CH_4^+ + CH_4 \rightarrow CH_5^+ + \cdot CH_3 \cdot$

REFERENCES AND NOTES

1. T. A. Lehman and M. M. Bursey, "Ion Cyclotron Resonance Spectrometry", John Wiley and Sons, New York, 1976.

2. J. I. Brauman and L. K. Blair, Ion Cyclotron Resonance Spectroscopy, in F. C. Nachod and J. J. Zuckerman (Eds.), Determination of Organic Structures by Physical Methods, Vol. 5, Academic, New York, 1976.

3. J. L. Beauchamp, Ion Cyclotron Resonance Spectroscopy, Ann. Rev. Phys. Chem. 22, 527 (1971).

4. M. B. Comisarow in "Advances in Mass Spectrometry", N. R. Daly (Ed.), Heyden and Son Ltd., London, 1978 and references therein.

5. R. T. McIver Jr., Rev. Sci. Instrum. 41, 555(1970).

6. Nicolet Instrument Corporation, Madison, Wisconsin.

7. The switching circuitry was built by Dr. Gérald Parisod.

8. J. L. Beauchamp and J. T. Armstrong, Rev. Sci. Instrum. 40, 123(1969).

9. The pulse sequence was developed with the aid of Valerio Grassi.

10. Valerio Grassi, M.Sc. Thesis, in preparation.

11. M. B. Comisarow, V. Grassi and G. Parisod, Chem. Phys. Lett. 57,413(1978).

12. James W. Cooper, "The Minicomputer in the Laboratory", John Wiley and Sons, 1977, pp. 248-255.

13. W. T. Huntress, J. B. Laudenslager and R. F. Pinizzotto, Int. J. Mass Spectrom. Ion Phys., 13, 331(1974).

III. DIGITAL TECHNIQUES AND THEIR APPLICATIONS TO FT-ICR

A. An Introduction to Problems With Discrete Analysis

i. Limited memory size

FT-ICR is a relatively new method for obtaining ICR spectra. Fundamental differences between FT-ICR and conventional ICR lead to different techniques for data acquisition and data reduction. It is the purpose of this chapter to discuss these techniques as applied to FT-ICR.

The generation of transient ICR signals has been discussed in Chapter 2. The acquisition of the transient signals which exist in FT-ICR must satisfy the Nyquist Sampling Theorem which states that the signal must be sampled at a rate which exceeds twice the band width of the signal. For an FT-ICR spectrometer operating at 20 kGauss, the cyclotron frequencies extend from about 1 MHz to 30 kHz for a mass range of m/e = 30 to 1000. Acquisition of this broad band signal requires a sampling rate of at least 2 MHz, much too fast for direct acquisition onto a magnetic disk. Hence, the number of data points that can be acquired is therefore restricted by the random access memory size of the computer.

Resolution in FT-ICR has been shown to be inversely proportional to mass and dependent upon the applied magnetic field as well as the computer memory available.[1] Therefore, acquisition of a broad band signal within the framework of limited memory size can lead to problems due to the lack of points to accurately describe spectral lineshapes. Accurate frequencies and intensities are mandatory for the

study of ion-molecule reactions.

ii, Discrete v. Continuous

In experimental practice, the continuous time domain response (i.e., the transient ICR signal) is not analytically transformed to produce a continuous frequency spectrum. Rather, the time domain response is sampled at a finite number of particular points in time to produce a discrete time domain response. The discrete time domain response is then numerically transformed to produce a discrete frequency spectrum.[2]

The discrete frequency spectrum is defined at M specific frequencies given by,

$$m/T \text{ Hz}, \quad m = 0, 1, 2 \cdots M \qquad (3\text{-}1)$$

where T is the acquisition time of the time domain signal. Clearly, the spacing in the discrete frequency spectrum is 1/T Hz. Unless the frequency to be determined happens to be exactly one of the particular frequencies given by equation 3-1, the intensities in the discrete frequency spectrum will not correspond to the peak maximum in the continuous frequency spectrum.

Figures 9 and 10 show two continuous lineshapes, A and B, where the maximum of A is exactly on one of the discrete frequencies of a discrete frequency spectrum and the maximum of B is half-way between the two discrete frequencies. Straight line connection of the amplitudes in the discrete frequency spectrum leads to the discrete lineshapes A' and B'.

Figure 9.

Continuous and discrete magnitude mode spectral peaks. Curves A and B are continuous spectral peaks of identical lineshape and intensity which were calculated from equation 3-5 with a value of $T/\tau = 1.0$. The maximum of Curve A falls exactly on one of the frequencies of the discrete frequency spectrum labelled n = 0. The maximum of Curve B falls exactly half way between two points of the discrete frequency spectrum labelled n = 0. Curves A' and B' are discrete frequency spectral lineshapes formed by straight line connection of the points in the discrete spectrum labelled n = 0. The discrete frequency spectrum labelled n = 1 has twice the resolution of the n = 0 discrete spectrum. The open circles are the values of Curve A in the n = 1 discrete spectrum.

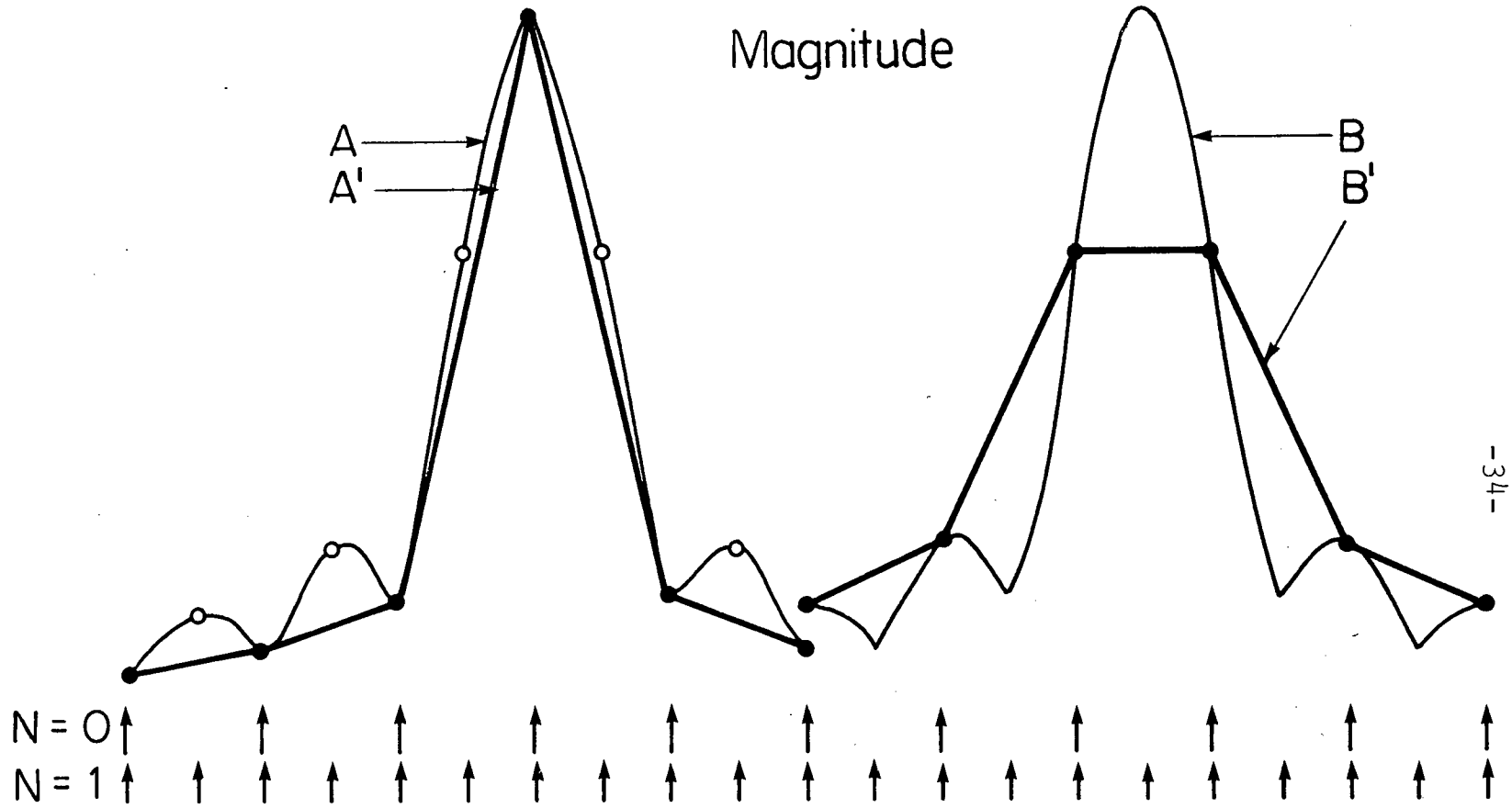

Figure 9.

Figure 10.

Continuous and discrete absorption mode spectral peaks. Curves A and B are continuous spectral peaks of identical lineshape and intensity which were calculated from equation 3-4 with a value of $T/\tau = 1.0$. The maximum of Curve A falls exactly on one of the frequencies of the discrete frequency spectrum labelled n = 0. The maximum of Curve B falls exactly half way between two points of the discrete frequency spectrum labelled n = 0. Curves A' and B' are discrete frequency spectral lineshapes formed by straight line connection of the points in the discrete spectrum labelled n = 0. The discrete frequency spectrum labelled n = 1 has twice the resolution of the n = 0 discrete spectrum. The open circles are the values of Curve A in the n = 1 discrete spectrum.

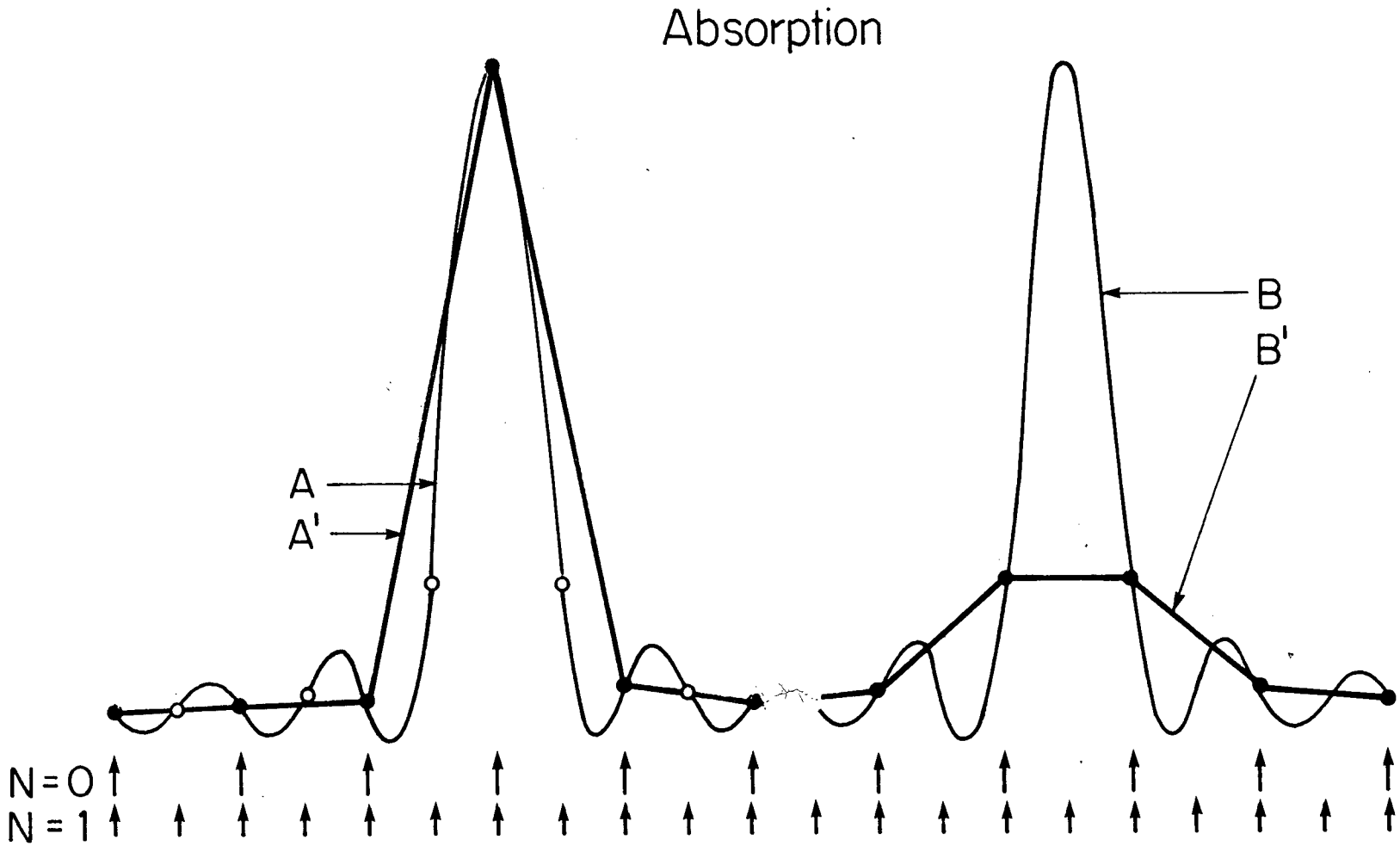

Figure 10.

It is obvious that A' provides an exact estimate of the amplitude and frequency of A. A' also provides a reasonable approximation to the linewidth of A. However, the amplitude, the frequency and the lineshape of B are poorly estimated by B'.

The problem illustrated in figs. 9,10 has been recognized in the literature. Two general solutions are available, curve fitting and using more points.

B. Solutions To The Discrete Points Problem

i. Curve Fitting

For cases in which the analytical lineshape is known in advance with only the location of the peak maximum and the intensity of the peak maximum being unknown, curve fitting techniques may be used to fit the few points in the vicinity of the peak maximum to the analytical lineshape. In this way, the peak maximum and frequency are obtained.

FT-ICR lineshapes are complex as shown by 3-4 and 3-5. The lineshape is determined by the value of T/τ where T is acquisition time and τ is the relaxation time of the transient ICR signal. τ is not the same for all peaks in a spectrum as τ is related to the mass of the ions in question. Therefore, a slightly different lineshape needs to be fit to each peak. This is a challenging problem that was not gone into deeply because preliminary calculations showed that fitting experimental points to FT-ICR lineshapes gives poor results[3] and other techniques are available that are of proven quality.

[illegible]

ii. Spectral Segment Extraction or Mixing

Spectral segment extraction techniques have been used previously to demonstrate the resolution achievable in FT-ICR.[4] In this procedure, the time domain FT-ICR signal is multiplied by a reference signal (i.e. mixing signal) to produce output signals at the sum and difference frequencies between the two input signals. This output signal is then passed through a low-pass filter which extracts just the difference frequency signal. The net effect of this process is to extract a band of ICR frequencies which are shifted down in frequency. Slower digitization rates are now possible due to the lower frequencies being sampled. As resolution is proportional to observation time, extremely high resolution is possible by using a reference frequency very close to the frequency of a particular ion. Figure 11 shows the HNO^-/CH_3O^- doublet formed from the dissociative attachment of thermal electrons to CH_3ONO at a pressure of $\sim 1 \times 10^{-9}$ Torr. The cyclotron frequencies of these ions in a 20 kGauss field are 990,543 Hz and 990,141 Hz respectively. By mixing the time-domain ICR signal from these ions with a frequency of 989 kHz and digitizing at 16 kHz , resolution of (M/ΔM 50%) 500,000 is obtained.

Mixing is the method of choice for observing ions that have similar cyclotron frequencies as extremely high resolution is possible. However, to obtain a spectrum covering a wide mass range, repeating this technique many times is neccessary, a process that is not used in practice.

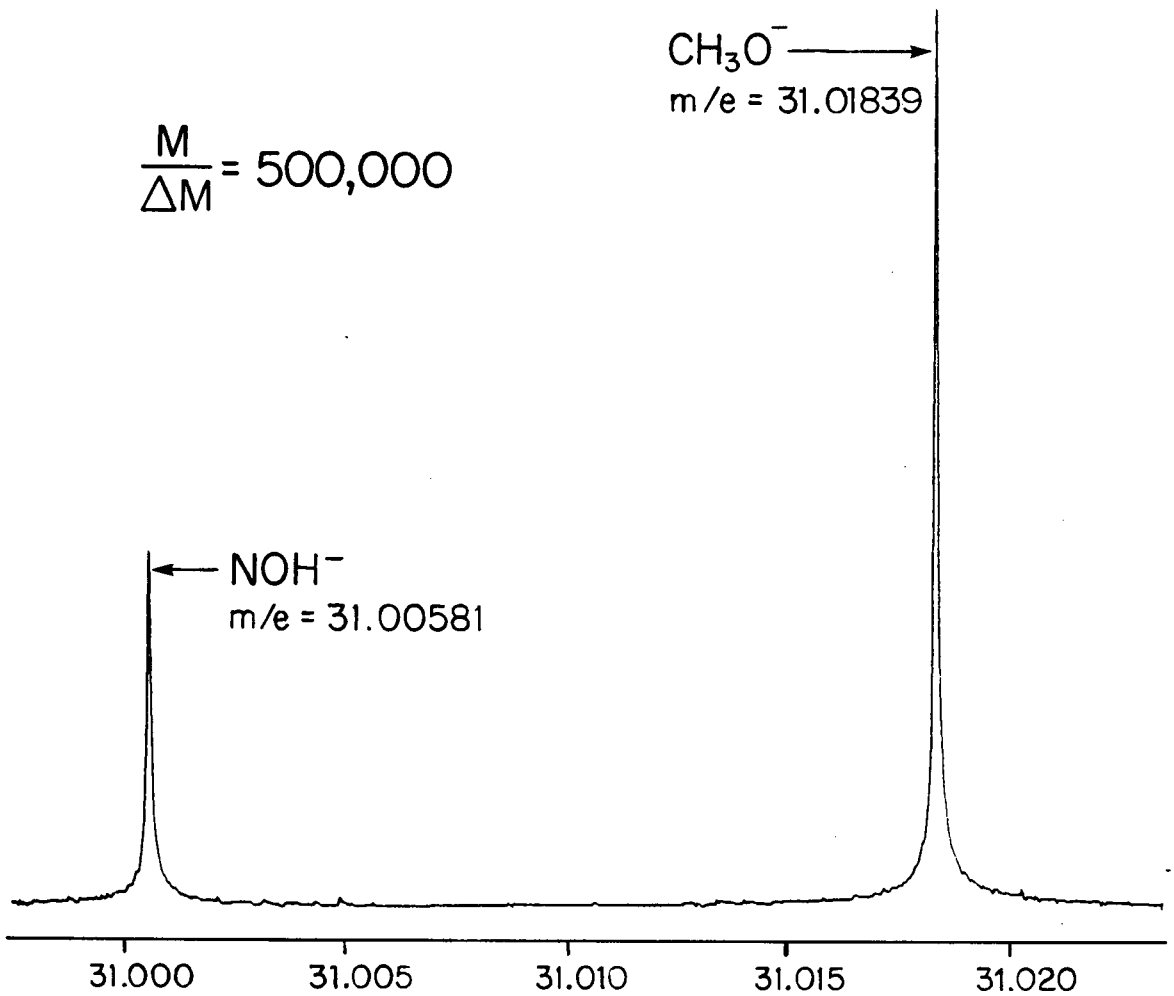

Figure 11 CH_3O^-/HNO^- doublet obtained using the "mixing" technique.

iii. Zero-filling

Another technique that has been found to be useful in many applications is zero-filling.[5-9] In this method, the time domain data table is extended by adding zeroes to the end of the sampled transient signal prior to Fourier transformation. Usually zeroes are added until the data table length has been extended by a factor of 2^n where n = 1, 2 · · ·, but this procedure is valid for any positive value of n.

In this way, the effective "zero-filled acquisition time", T_z, is now longer and the spacing in the discrete frequency spectrum is now reduced to $1/T_z$ from 1/T.

$$T_z = T \times 2^n \qquad (3\text{-}2)$$

In the limit, $n \rightarrow \infty$, the numerical Fourier transform becomes identical to the analytical Fourier transform and the discrete frequency spectrum becomes identical to the continuous frequency spectrum.

A further advantage of this interpolation method is that the first set of added zeroes increases the signal to noise ratio of the final absorption mode spectrum.[5] Further zero-fillings will only interpolate to the correct lineshape. It is the correct lineshape that is desired in FT-ICR experiments so the point of how much zero-filling is needed will be pursued in some detail.

C. Accuracy Obtained by Zero-filling

i. Intensities

While the effect of zero-filling has been known for quite some time, we are unaware of quantitative criteria for determining the number of zero-fillings which is required for a particular accuracy. This criterium is required for FT-ICR experiments because accurate intensities and frequencies are crucial to the success of an experiment.

Determination of the error resulting from finite zero-filling of Fourier transform faradaic admittance data has recently been examined by Smith.[8] However, no guidelines were given for general applications of this technique. Also, Horlick has shown the error in peak maximum measurements as a function of the number of points above the half-maximum for various lineshapes.[7] We will derive here expressions for the accuracy of peak maximum determination as a function of T/τ. That is, the only parameter required is how much the time domain signal has decayed during the observation time.

Consider a continuous time domain signal of the form

$$F(t) = \exp(-T/\tau)\cos\omega t \quad 0 < t < T \tag{3-3}$$

The continuous absorption mode frequency spectrum (i.e. the analytical Fourier transform) of 3-3 is[11]

$$A(\Delta\omega) = \frac{\tau}{1+(\Delta\omega)^2\tau^2}\left(1+\exp(-T/\tau)\left((\Delta\omega)\tau\sin((\Delta\omega)T)-\cos((\Delta\omega)T)\right)\right) \tag{3-4}$$

The continuous magnitude mode frequency spectrum of 3-2 is[11]

$$C(\Delta\omega) = \left(\frac{\tau^2}{1+(\Delta\omega)^2\tau^2}\right)^{\frac{1}{2}}\left(1-2\exp(-T/\tau)\cos((\Delta\omega)T)+\exp(-2T/\tau)\right) \quad (3\text{-}5)$$

In equations 3-3 to 3-5, τ is the relaxation time of the signal, $\Delta\omega$ is the frequency distance from the maximum ($\Delta\omega=\omega-\omega'$ where ω' is the frequency at the peak maximum) and T is the time over which the signal was observed. Equations 3-3 to 3-5 are very general equations and are applicable to many forms of spectroscopy and in particular to ICR and NMR.

Now, when 3-3 is sampled at a series of discrete times, the discrete frequency spectrum resulting from Fourier transformation will exist only at the particular frequencies given by 3-1. Thus, the only allowed values for the distance between the points in the discrete frequency spectrum are given by

$$\Delta f = 1/T \quad (\text{Hz}) \qquad (3\text{-}6)$$

if no zero-filling is done prior to Fourier transformation, and by

$$\Delta f = 1/T_z = \frac{1}{2^n T} \quad (\text{Hz}) \quad n = 0, 1, 2 \cdots \qquad (3\text{-}7)$$

if the time domain signal is zero-filled n times prior to Fourier transformation.

For a continuous spectral peak which happens to fall exactly on one of the discrete frequencies of the discrete frequency spectrum, as curve A in figures 9 and 10, the intensity of the lineshape will be defined only at the discrete frequency values given by

$$\Delta\omega = \frac{2\pi N}{2^n T} \qquad N = \pm 0, 1, 2 \cdots \tag{3-8}$$

where n is the number of zero-fillings. For a value of N = +1, the intensity of the peak at the first discrete frequency above the peak maximum will be obtained. Substituting equation 3-8 with a value of N = +1 into 3-4 gives

$$A(\Delta\omega) = \tau\left(1+\frac{Y}{X}\right)^{-1}\left(1+e^{-Y}\left(\frac{Y}{X}\sin(Y)-\cos(Y)\right)\right) \tag{3-9}$$

where

$$X = T/\tau \tag{3-10}$$

and

$$Y = \frac{2\pi}{2^n} \tag{3-11}$$

Equation 3-9 gives the discrete intensity value for the first discrete frequency above the peak maximum (i.e. N = +1) for an absorption mode lineshape as a function of X, the ratio of the acquisition time T, to the relaxation time τ, and n, the number of zero-fillings. Equation 3-12 is the corresponding expression for a discrete magnitude lineshape.

$$C(\Delta\omega) = \tau\left(1+(Y/X)^2\right)^{-\frac{1}{2}}\left(1-2\exp(-X)\cos(Y)+\exp(-2X)\right) \tag{3-12}$$

Examination of figure 9 leads to a systematic procedure for determining the maximum amplitude error due to the finite frequency resolution of a discrete frequency spectrum. Curve A in figure 9 is a continuous mode lineshape calculated from 3-3 for $T/\tau = 1.0$. Curve B in figure 9 is a continuous lineshape which is identical to Curve A but is at a different

frequency. If peak A was obtained by sampling a time domain signal and Fourier transformation, and if the maximum of Curve A was exactly on one of the points in the discrete frequency spectrum, the discrete magnitude mode lineshape obtained by connecting the points in the discrete frequency spectrum would be A'. If the sampling conditions were appropriate for Curve A, then the maximum of Curve B would be incorrectly indicated by the discrete magnitude lineshape, Curve B'. Figure 10 is the same as figure 9 except that absorption mode lineshape is used.

If the transient which leads to Curve A was zero-filled once (n=1) prior to Fourier transformation, the points indicated as open circles in figure 9 (and 10) would be obtained for spectral peak A. Since the maximum for the continuous peak B falls exactly half-way between two of the discrete frequencies of the non zero-filled (n=0) discrete frequency spectrum, measurement of spectral peak B' will lead to the worst possible estimate for the frequency and the amplitude of Curve B. If peak B was less than half-way between two frequencies of the n=0 discrete spectrum, B' would have an amplitude closer to that of Curve B. Comparison of Curve B' with the open circles of Curve A leads to the following conclusion: The minimum amplitude for a peak which falls between two points of a non zero-filled spectrum will be equal to the amplitude of the first (N=1) point away from the maximum of the "zero-filled once" (n=1) spectrum of a peak

whose maximum falls exactly on one of the frequencies of the non zero-filled (n=0) spectrum. The preceeding statements may be generalized to:

$$\left(\begin{array}{l}\text{Maximum relative error}\\ \text{obtained after n}\\ \text{zero-fillings}\end{array}\right) = \left(1.0 - \frac{\text{equation 3-12 (n=n+1)}}{\text{equation 3-12 (n=}\infty\text{)}}\right) \qquad (3\text{-}13)$$

and

$$\left(\begin{array}{l}\text{Maximum relative error}\\ \text{obtained after n}\\ \text{zero-fillings}\end{array}\right) = \left(1.0 - \frac{\text{equation 3-9 (n=n+1)}}{\text{equation 3-9 (n=}\infty\text{)}}\right) \qquad (3\text{-}14)$$

Equation 3-13 gives the maximum relative error for a magnitude mode lineshape as a function of n and T/τ. Equation 3-14 is the corresponding absorption mode expression. Equations 3-13,14 depend upon the ratio T/τ but are independent of the absolute values of T and τ.

Figure 12 shows the percentage amplitude error resulting from finite zero-filling for the absorption mode lineshape. As expected, the error is rapidly reduced by extended zero-filling prior to Fourier transformation. As the time domain signal is relaxed during the acquisition time (increasing T/τ), the magnitude of the amplitude error for fixed n also becomes less.

Figure 13 shows the percentage amplitude error for the magnitude mode lineshape. The dependence upon n and T/τ is the same as in the case for the absorption mode. However, the amplitude error for the magnitude mode is less for any

Figure 12.

Relative error due to noninfinite zero-filling for an absorption mode lineshape. Each curve gives the maximum percentage error for a particular ratio of T/τ as a function of the number of zero-fillings. The error at integral values of n is the most important but the curves are valid for nonintegral values of n also. The curves were calculated from equation 3-14. Note that the error scale is different than that of figure 13.

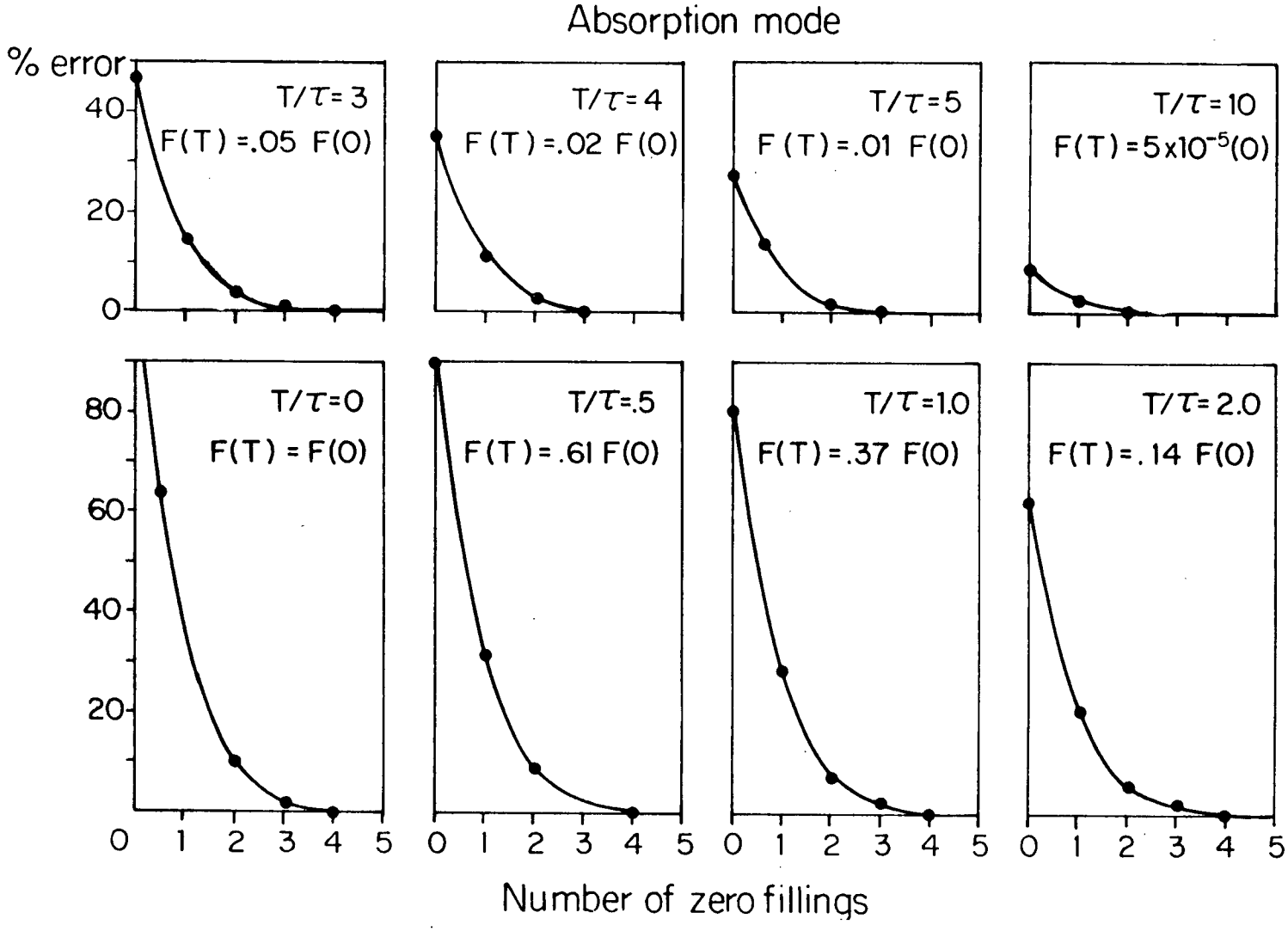
Absorption mode
% error
40
20
0
T/τ = 3
F(T) = .05 F(0)
T/τ = 4
F(T) = .02 F(0)
T/τ = 5
F(T) = .01 F(0)
T/τ = 10
F(T) = 5x10⁻⁵(0)
80
60
40
20
T/τ = 0
F(T) = F(0)
T/τ = .5
F(T) = .61 F(0)
T/τ = 1.0
F(T) = .37 F(0)
T/τ = 2.0
F(T) = .14 F(0)
0 1 2 3 4 5
Number of zero fillings

Figure 12.

Figure 13.

Relative error due to noninfinite zero-filling for a magnitude mode lineshape. Each curve gives the maximum percentage error for a particular ratio of T/τ as a function of the number of zero-fillings. The error at integral values of n is the most important but the curves are valid for nonintegral values of n also. The curves were calculated from equation 3-13. Note that the error scale is different than that of figure 12.

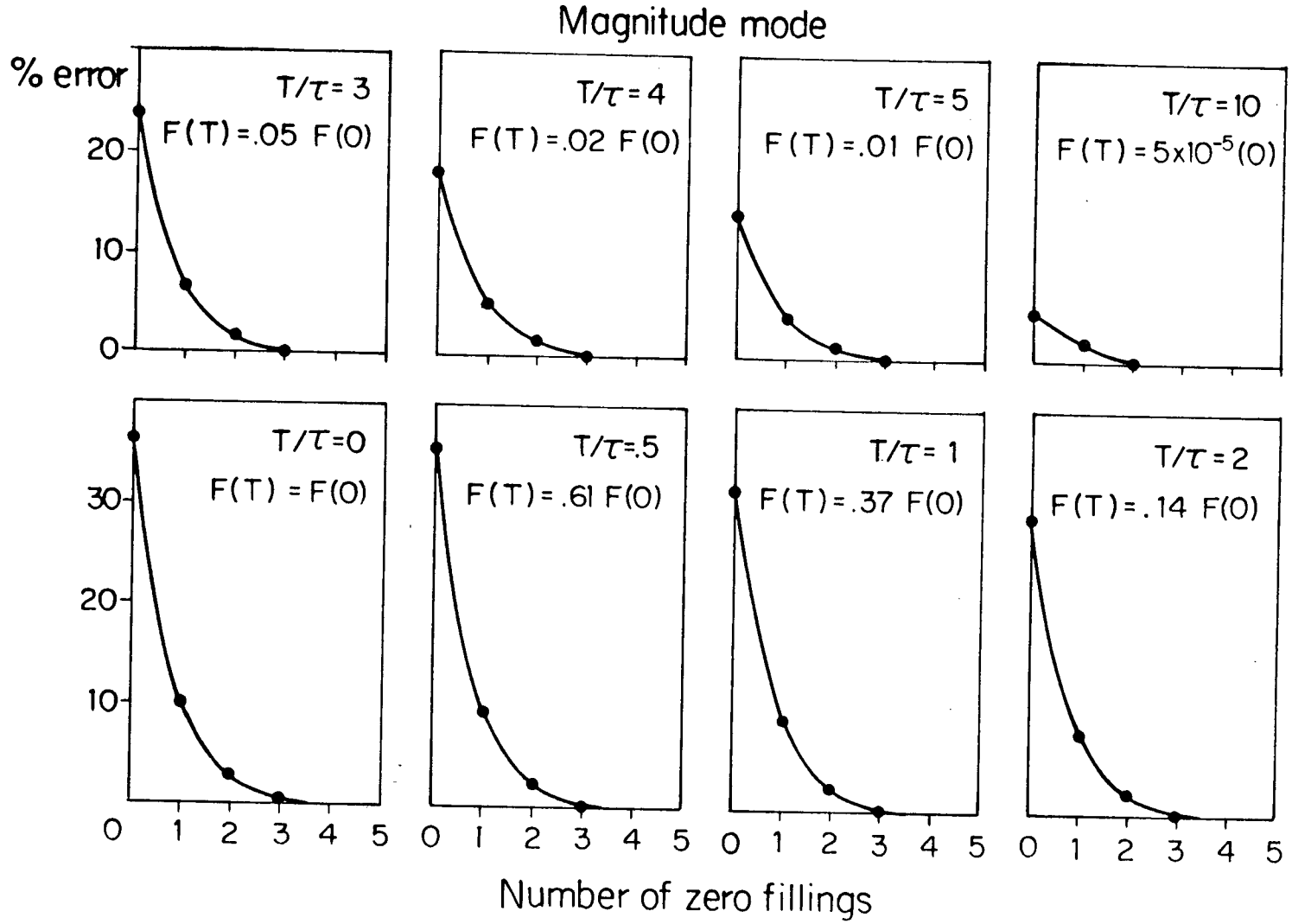
Magnitude mode
% error
T/τ = 3
F(T) = .05 F(0)
T/τ = 4
F(T) = .02 F(0)
T/τ = 5
F(T) = .01 F(0)
T/τ = 10
F(T) = 5x10⁻⁵(0)
T/τ = 0
F(T) = F(0)
T/τ = .5
F(T) = .61 F(0)
T/τ = 1
F(T) = .37 F(0)
T/τ = 2
F(T) = .14 F(0)
0
10
20
30
0 1 2 3 4 5
Number of zero fillings

Figure 13.

given values of n and T/τ than for the absorption mode. This is because the magnitude lineshape is broader than the absorption lineshape.

One general conclusion which follows directly from figures 12 and 13 is that three zero-fillings are enough to decrease the amplitude error to a few per cent for undamped transients. For more damped transients, less zero-filling is neccessary.

ii. Frequencies

Acquisition time, T, is related to the dwell time, DW, or the time that the digitizer spends on each point and the number of points to be acquired, #pts., by the formula

$$T = DW \times \#pts. \qquad (3\text{-}15)$$

where DW is in sec/point. Substituting 3-15 into 3-6 yields

$$\Delta f = \frac{1}{DW \times \#pts} \qquad (3\text{-}16)$$

The number of real points in the frequency domain is #pts/2 because the Fourier transform algorithm used produces both real and imaginary coefficients even if all the data is real.[10] Equation 3-15 now becomes

$$\Delta f = \frac{1}{2 \times DW \times \#pts} \qquad (3\text{-}17)$$

in practice. $\Delta f/2$ is therefore the maximum error in the frequency determination of a peak.

Figure 14 shows a plot of mass v. ΔM for various dwell times where mass is in amu and ΔM is the maximum error in mass determination as found from

Figure 14.

Plot of mass v. ΔM for various values of DW. The curves were calculated from equation 3-18 where it is assumed that B = 20 kGauss and #pts = 16k. DW is in μsec/point.

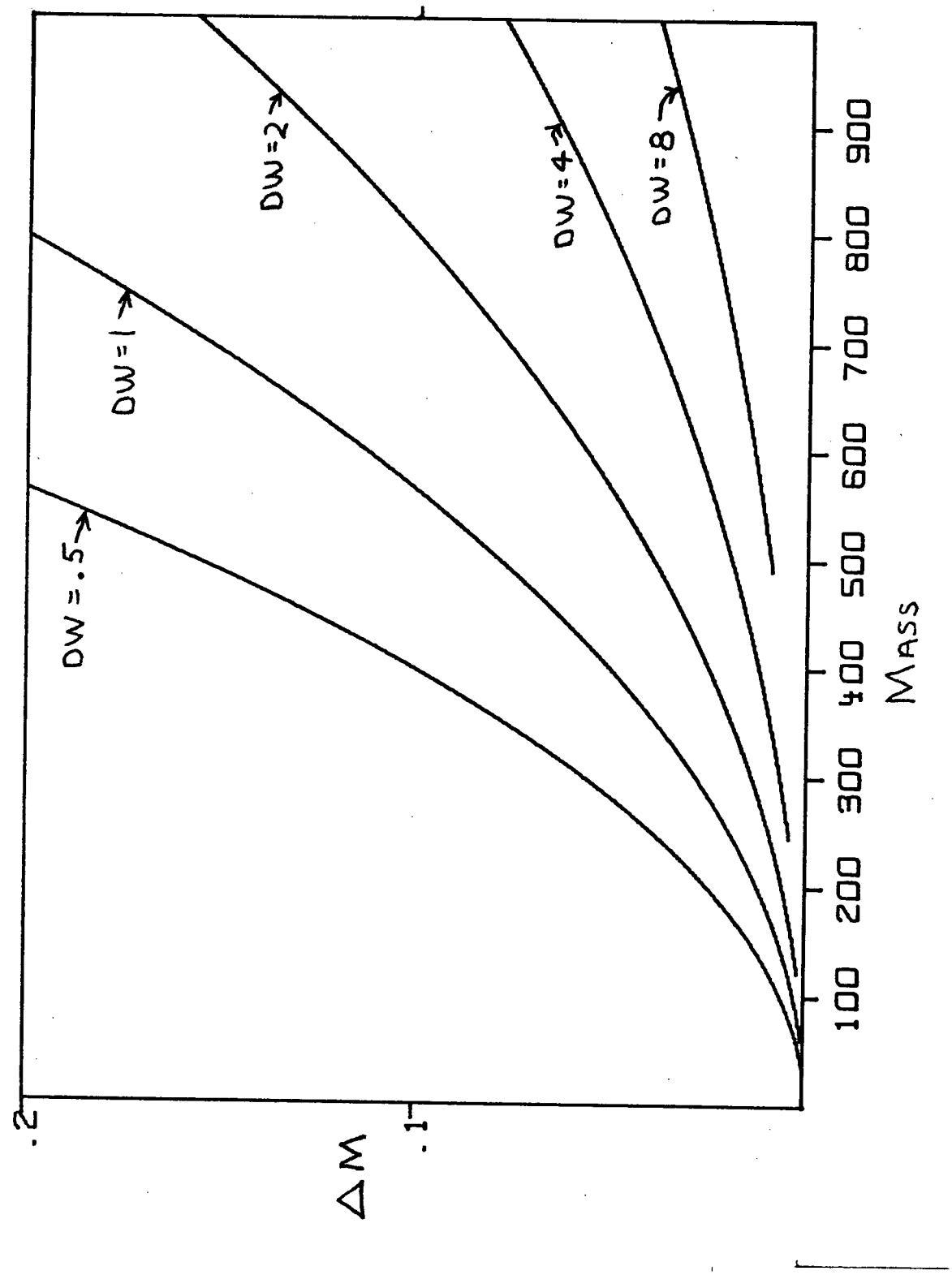
.2
.1
ΔW
DW=.5
DW=1
DW=2
DW=4
DW=8
100 200 300 400 500 600 700 800 900
MASS

$$\Delta M = 1.037 \times 10^{-7} \, (m^2/qB)\Delta f \qquad (3\text{-}18)$$

where B is in kGauss, q is in multiples of elementary charge and m is mass in AMU.[11] Figure 14 was obtained assuming direct acquisition of signal, i.e. no mixing. It is seen that when DW is low (high sampling rate), the error in mass determination at the high mass end of the scale becomes excessive. By using higher values of DW (lower sampling rate), ΔM can be reduced, but only at the expense of mass range. Fortuneately, zero-filling can be used in such a way that allows a broad band spectrum to be recorded in one experiment that gives acceptable values for ΔM.

Combining 3-7 and 3-15 yields

$$\Delta f = \frac{1}{2 \times DW \times \#pts \times 2^n} \qquad (3\text{-}19)$$

where n is a positive integer equal to the number of times the original data set was extended by a factor of two with zeroes prior to Fourier transformation. Figure 15 shows the effect of zero-filling on ΔM for the case where DW is held constant. By comparing figures 14 and 15, it is apparent that zero-filling and increasing DW have the same effect on ΔM with the important difference that with zero-filling the mass range can be held constant at any value.

It must be emphasized that while zero-filling can improve ΔM, the accuracy of mass determination, it can not improve resolution. Resolution enhancement can only be achieved by observing the transient for a longer time. A

Figure 15.

Plot of mass v. ΔM for various values of n where n = number of zero-fillings. The curves were calculated from equation 3-18 where it is assumed that B = 20 kGauss, #pts = 16k and DW is constant at .5 μsec/point.

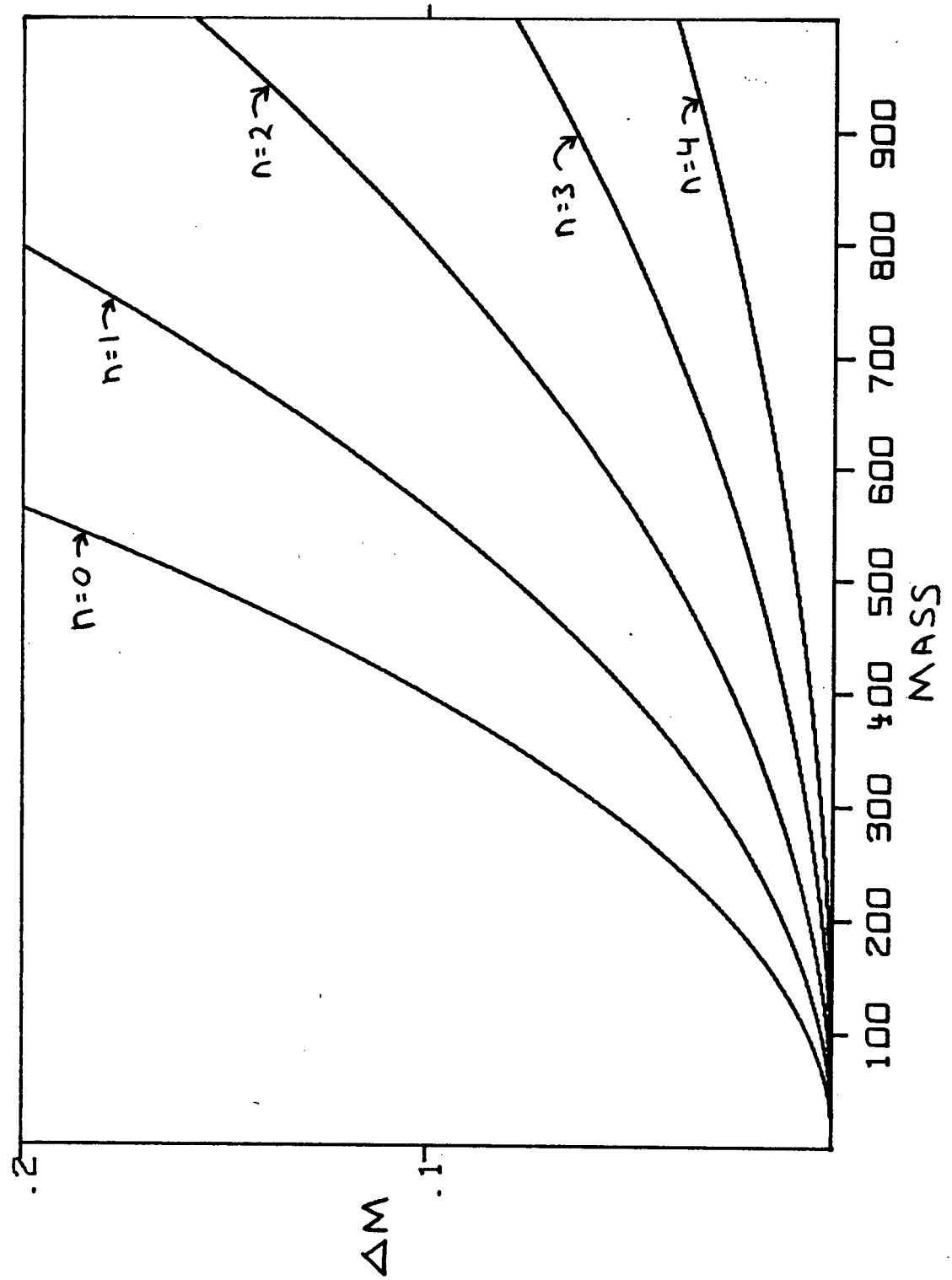
n=0
n=1
n=2
n=3
n=4
.2
.1
ΔM
100 200 300 400 500 600 700 800 900
MASS

program written at Nicolet Instrument Corporation called DNMR allows us to do disk based Fourier transforms of 512 k words.[12] This allows us to extend a 16k data set by a factor of 2^5 or zero-filling 5 times.

D. Leakage

One problem that is encountered with zero-filling is the appearance of side bands on peaks when a transient that has not decayed 100% is extended by zeroes.[13] The appearance of these side bands is commonly referred to as leakage in the spectrum. These side lobes are not caused by zero-filling, they exist due to truncation of the transient. However, since the Fourier transform process produces both real and imaginary parts, the points that define the side lobes seem to be missing unless one power-of-two of zero-filling is used to recover them. This is readily seen in figure 9 where the open circles represent points that are obtained after zero-filling once. It is seen that with the addition of these points, side lobes have appeared that were not visible in the unfilled spectrum.

It is neccessary to reduce leakage in FT-ICR experiments as small peaks in the vicinity of larger peaks can easily be lost in the leakage. Various window functions such as Hanning, exponential and trapezoidal are available in software packages to reduce leakage. Application of a Hanning window function prior to extension of the data set by zeroes has been found to reduce leakage in FT-ICR experiments to acceptable levels.[14] There is some line broadening with this window

function but the leakage is removed and the peak intensities have the same relative values.

Figure 16 shows a broad band spectrum of tris(perfluoroheptyl)-s-triazine obtained by extension of the original 16k data set to 128k with zeroes prior to Fourier transformation. The base peak at m/e=866 has been expanded to show the effect of leakage more clearly. All peaks in figure 16 have bothersome side lobes but they are not readily apparent at low masses because figure 16 is plotted on a mass scale, not a frequency scale. Hence, frequencies are compressed at the low mass end of the spectrum and the leakage is not seen there unless the scale is expanded. The peak at m/e=69 is also expanded in figure 16 to show that the effect of leakage is inherent throughout the spectrum. Figure 17 was obtained in exactly the same manner as figure 16 except for the application of a Hanning window function prior to zero-filling. Again, the peak at m/e=866 is expanded but the leakage is removed by the window function.

E. Selective Zero-filling

High orders of zero-filling can reduce ΔM to an acceptable minimum but long disk based Fourier transforms are very time consuming. For example, a 16k transform takes 14 seconds, 64k takes 4 minutes while 512k takes over 50 minutes! Since the problem of mass determination occurs at the high mass end of the scale, it would be advantageous to be able to zero-fill only this portion of the spectrum for accurate mass determination. Following the method of Pajer and

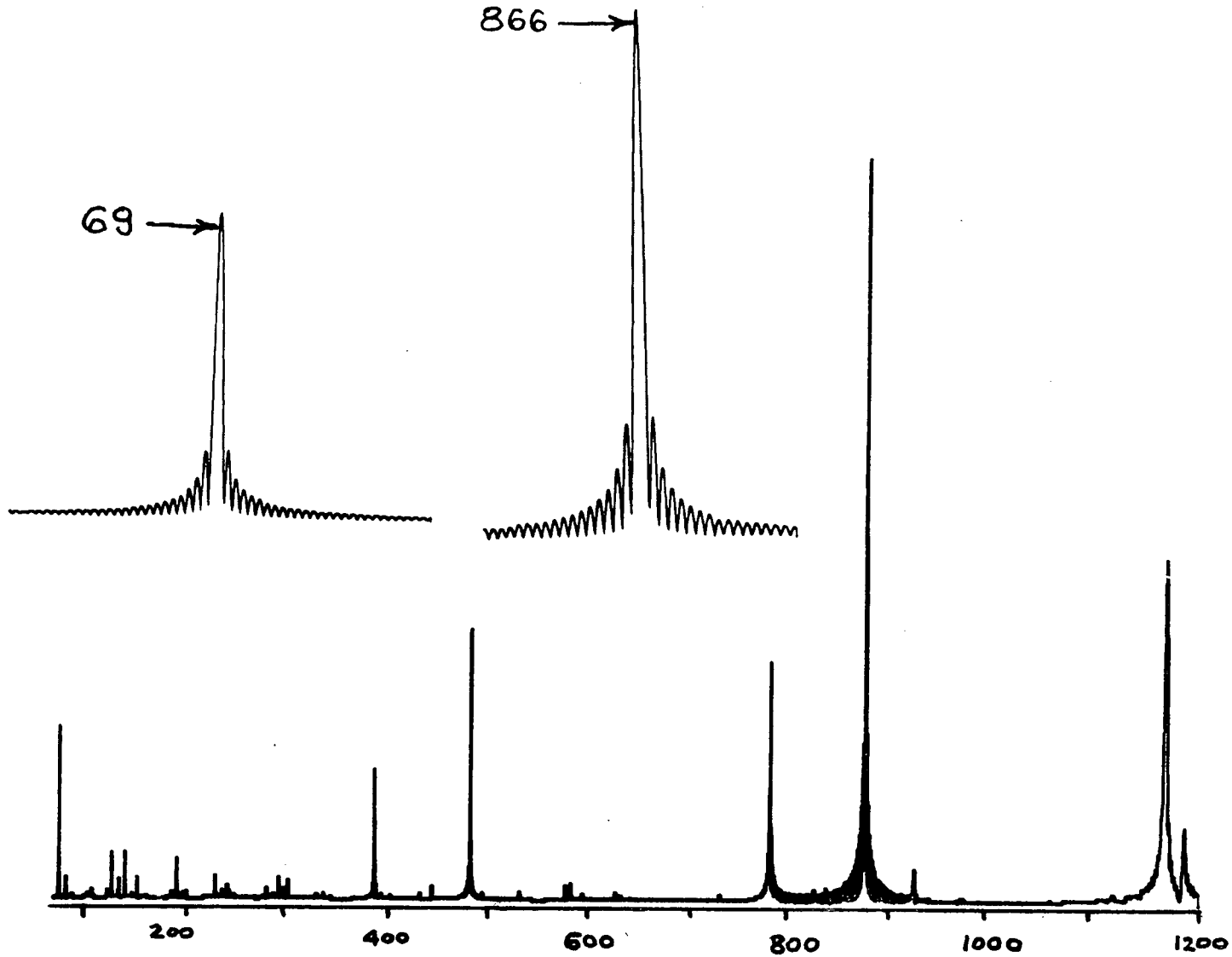

Figure 16 Wide band spectrum of tris(perfluoroheptyl)-s-triazine.
Original 16k data set expanded to 128k before Fourier transformation.

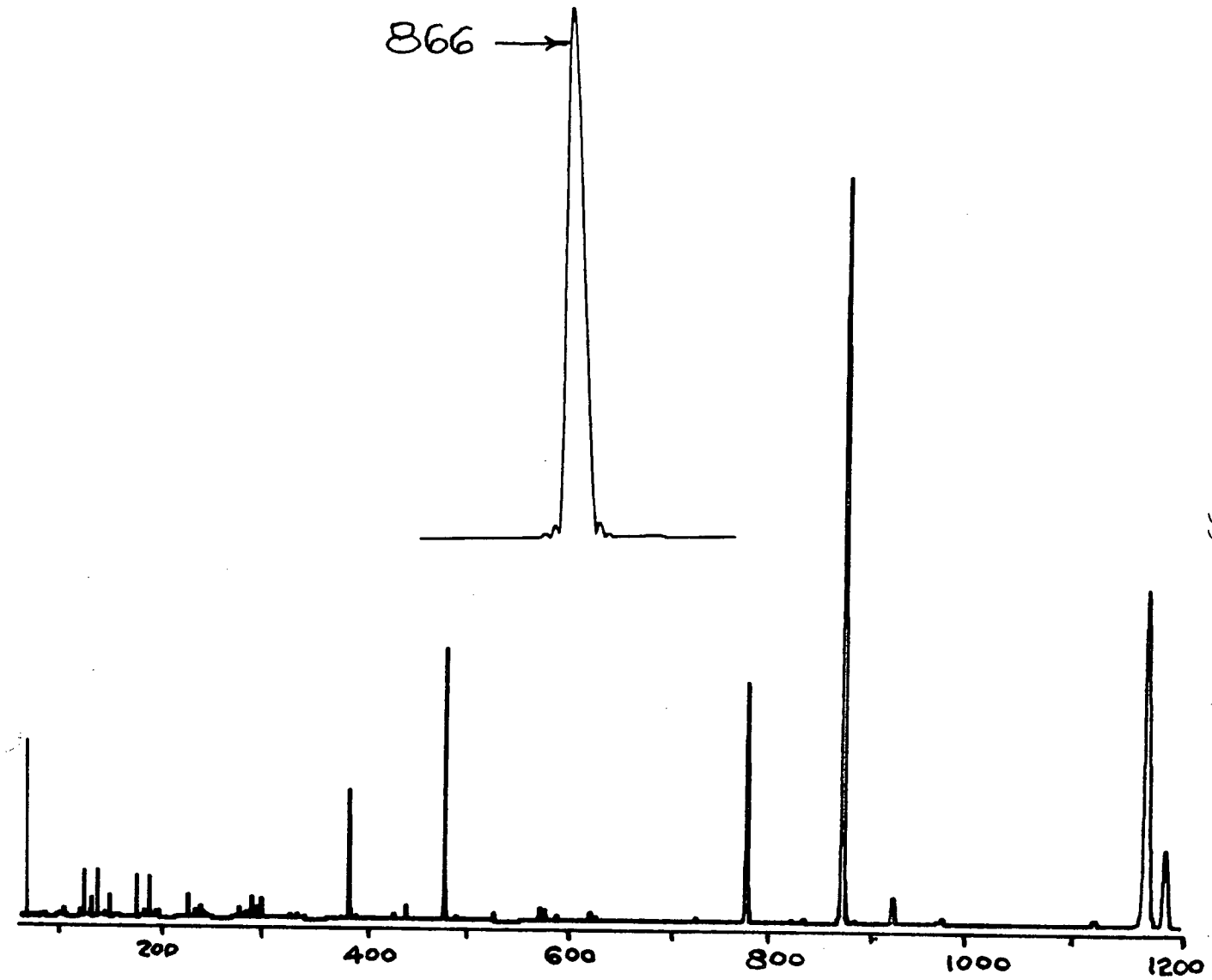

Figure 17 Hanning window function applied to transient of figure 16.

Armitage it is possible to selectively zero-fill using the following procedure: collect data and Fourier transform as usual to obtain a frequency domain spectrum, save only the desired high mass segment (or any other segment for that matter) with its associated imaginary part, Fourier transform this back to the time domain then zero-fill to the desired amount before finally Fourier transforming back to the frequency domain.[15] Figure 18 shows how this method was used to selectively fill the high mass portion of figure 16. The original 16k transient was Fourier transformed to yield a frequency domain spectrum. Then, 1k real and 1k imaginary points corresponding to the high mass end of the spectrum were selected and transformed back to the time domain to yield a 2k transient. This transient was zero-filled to 16k and finally Fourier transformed to give figure 18. Thus, the segment corresponding to mass 491-∞ was selectively zero-filled. Figure 19 is the unfilled spectrum shown for comparison. Note the difference in lineshapes between the two examples and how the peak position is more readily apparent in figure 18.

This is a powerful technique as it allows for a broad band spectrum to be collected and analyzed segmentally or wholly, but unlike the mixing technique only one experiment needs to be done. Of course resolution is not as high as it can be by using the mixing technique.

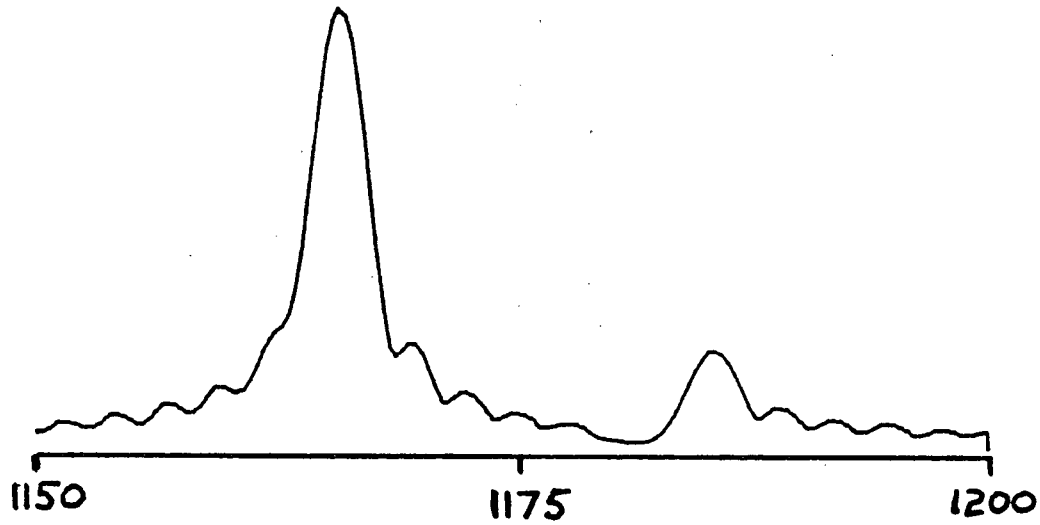

Figure 18 High mass portion of figure 16 obtained using the selective filling technique of Armitage and Pajer.

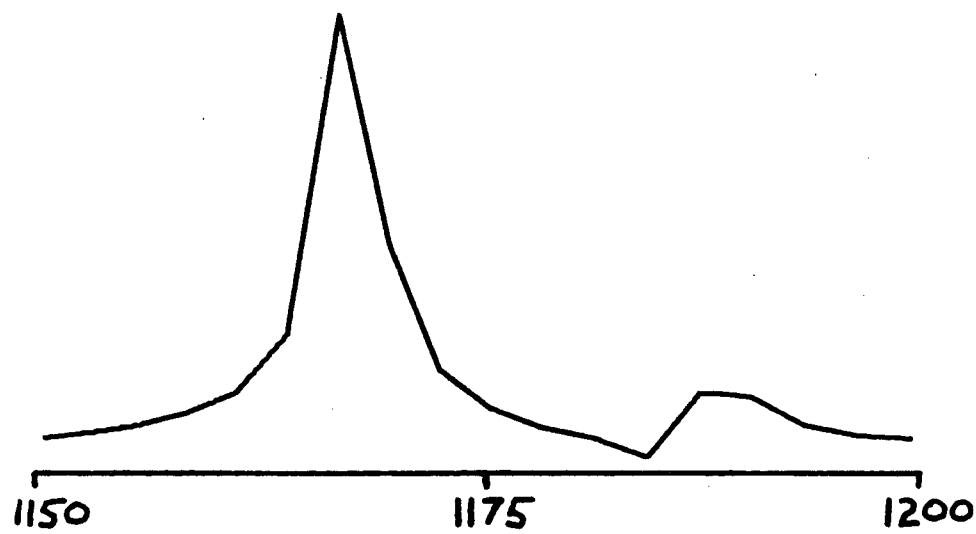

Figure 19 Unfilled high mass portion of figure 16.

F. Mass Calibration

As a Fourier transformation of a time domain ICR signal produces a frequency domain spectrum, an accurate method must be available for converting frequencies to masses. Beauchamp and Armstrong have derived the following expression for the frequency of an ion in a crossed electric and magnetic field[16]

$$\omega^2 = \frac{qH}{mc}^2 - \frac{4qV}{md^2} \qquad (3\text{-}20)$$

In equation 3-20, ω is frequency, V is the trapping voltage, d is the distance between the top and bottom plates of the ICR cell, q is the charge on the ion, H is magnetic field, c is the speed of light and m is mass of the ion. Equation 3-20 can be solved for m/q and after introduction of the parameters $A=(H/c)^2$ and $B=4V/d^2$, the following expression due to McIver is obtained[17]

$$\frac{m}{q} = \frac{-B + (B^2 + 4A\omega^2)^{\frac{1}{2}}}{2\omega^2} \qquad (3\text{-}21)$$

Once A and B are known, all that is required for the mass determination of an ion is the frequency of that ion. A and B are determined by using two known mass values and their experimental frequencies to solve equation 3-21.

Table 2 gives the major ions seen in figure 16 and experimentally determined frequencies. Also included are the calculated and actual masses and deviations for each ion. Various combinations of masses have been used for the fitting

Table 2 Calibration Data for the FT-ICR Spectrometer

ION	EXACT m/q	FREQUENCY Hz	CALCULATED[a] m/q	ERROR	CALCULATED[b] m/q	ERROR	CALCULATED[c] m/q	ERROR
CF_3^+	68.9952	454148	68.9952	0.000	68.9952	0.000	68.9952	1.9788E-5
$C_2F_5^+$	118.9920	263183	118.989	-0.003	118.992	0.000	118.991	2.3932E-4
$C_3F_5^+$	130.9920	239037	130.991	0.000	130.995	0.003	130.994	-2.0599E-3
$C_3F_7^+$	168.9888	185219	168.979	-0.010	168.986	-0.003	168.984	4.0564E-3
$C_8F_{14}N^+$	375.9807	83053.8	375.950	-0.030	375.998	0.017	375.984	-3.8061E-3
$C_{10}F_{17}N_2^+$	470.9790	66230.7	470.930	-0.049	471.009	0.030	470.986	-6.9742E-3
$C_{16}F_{29}N_2^+$	770.9598	40321.4	770.856	-0.104	771.083	0.123	771.020	-6.0129E-2
$C_{18}F_{32}N_3^+$	865.9582	35865.7	865.668	-0.290	865.958	0.000	865.877	0.08085
$C_{24}F_{44}N_3^+$	1165.9390	26542.7	1165.64	-0.299	1166.18	0.241	1166.03	-0.09371
$C_{24}F_{45}N_3^+$	1184.9374	26100.2	1185.13	0.193	1185.69	0.753	1185.53	0.39940

[a] m/q=68.9952 and 130.9920 used to fit eq. 3-21. [b] m/q=68.9952 and 865.9582 used to fit eq. 3-21. [c] All points fit to eq. 3-21 to find best values of A and B.

of equation 3-21 with good success. Mass calibration by FT-ICR is seen to be quite good when compared to previous ICR calibrations. For example, McIver measured the mass of $C^{35}Cl_2{}^{37}Cl^+$ (m/q=118.903) as 118.887 for an error of .016 amu. We have measured the mass of a similar ion $C_2F_5^+$ (m/q=118.992) as 118.989 or an error of .003 amu. Also, the mass range has been extended to at least 1200 whereas previous ICR experiments have been limited to less than m/q=400 with poor resolution.

Good accuracy is obtained by this mass calibration method but it is not possible to identify different isobaric ions in a broad band spectrum solely by mass because: 1) An inordinate number of points must be transformed to determine frequencies to a high degree of accuracy. 2) The equation of motion of ions in a cubic trapped ion cell is not known so the use of equation 3-20 is questionable, although Table 2 shows it to be reasonably accurate. 3) The effect that ions have on each others' frequencies due to induced magnetic fields and space charges can not be predicted. 4) Variations of the applied magnetic field during experiments and field inhomogeneities can cause loss of resolution.

Methods have been presented for obtaining FT-ICR spectra. It has been shown that there is a play-off between resolution, mass range and computational time required when performing FT-ICR experiments. In practice, this play-off is not

serious as asset of satisfactory acquisition parameters can usually be found that allow the experiment to be performed in an efficient manner. Also, data acquisition and processing are under computer control allowing for large amounts of data to be acquired and analyzed fairly quickly.

REFERENCES AND NOTES

1. M. B. Comisarow and A. G. Marshall, J. Chem. Physics 64, 110(1976).

2. E. O. Brigham, "The Fast Fourier Transform", Prentice-Hall, Inc., Englewood Cliffs, New Jersey, 1974, pp. 132-146.

3. Valerio Grassi, private communication.

4. M. B. Comisarow, G. Parisod and V. Grassi, proceedings of 26th ASMS meeting, St. Louis, MO., 1978, paper RD5.

5. E. Bartholdi and R. R. Ernst, J. Mag. Resonance 11, 9(1973).

6. P. R. Griffiths, Appl. Spectrosc. 29, 11(1975).

7. G. Horlick and W. K. Yuen, Anal. Chem. 48,1643(1976).

8. R. J. O'Halloran and D. E. Smith, Anal. Chem. 50, 1391(1978).

9. M. Forker and J. D. Rogers, Nucl. Instrum. and Methods 96, 453(1971).

10. J. W. Cooper, "The Minicomputer in the Laboratory", Wiley, New York, 1977, pp. 261-294.

11. M. B. Comisarow and A. G. Marshall, unpublished results.

12. Nicolet Instrument Corporation, 5225 Verona Rd., Madison, Wisconsin.

13. reference 2, pp. 140-146.

14. The window functions used are provided in Lab-1180 General Signal Averaging Package, Nicolet Instrument Corp., 5225 Verona Rd., Madison, Wisconsin.

15. R. T. Pajer and I. M. Armitage, J. Mag. Resonance 21, 485(1976).

16. J. L. Beauchamp and J. T. Armstrong, Rev. Sci. Instrum. 40, 123(1969).

17. E. B. Ledford and R. T. McIver, Int. J. Mass Spectrom. Ion Phys. 22, 399(1976).

IV. THE GAS PHASE REACTIONS OF CARBONATES

A. A Brief Review of Previous Ester Studies

The attack of a nucleophilic reagent at a carbonyl center is a common feature of many organic reactions and thus has been actively studied by many investigators.[1] The mechanistic details of many solution processes such as ester hydrolysis are well understood. However, recent gas phase work has shown that it is still not known how the intrinsic properties of the reagents affect the outcome of the reaction. Attempts to improve the knowledge of chemical reactions have concentrated on two areas: theoretical approaches and re-creating solution processes in the gas phase where the role of the solvent is eliminated. This chapter is concerned with the latter approach as studied by FT-ICR.

A classic solution experiment utilizing ^{18}O labelling showed that the alkaline saponification of amyl acetate proceeds by breakage of the acyl-oxygen bond.[2] Overwhelming evidence by Bender showed that the reaction involves the initial formation of a tetrahedral intermediate from the addition of OH^- to the carbonyl group.[3] His evidence was based upon the alkaline hydrolysis of ethyl benzoate which was labelled with ^{18}O in the carbonyl oxygen. The reaction was stopped before completion and analysis showed some ^{16}O in the carbonyl oxygen, evidence for the equivalence of oxygens in an intermediate. This is commonly called a $B_{AC}2$ process or simply a tetrahedral mechanism. The corresponding mechanism, whereby the alkyl-oxygen bond is broken is less

common. This is an S_N2 or $B_{AL}2$ process and is rare being known mainly for methyl and ethyl esters reacting with powerful nucleophiles.[4]

Various research groups have studied the reactions of negative ions with esters in the gas phase and have found that several mechanisms become competitive in the absence of a solvent.[5-12] Notable has been the work of Riveros[8] who studied the reactions of F^- with alkyl acetates and propionates and concluded: (1) S_N2 processes are important in the gas phase reactions of some esters and (2) esters containing β hydrogens lead to different products than methylesters due to the addition of an elimination type reaction

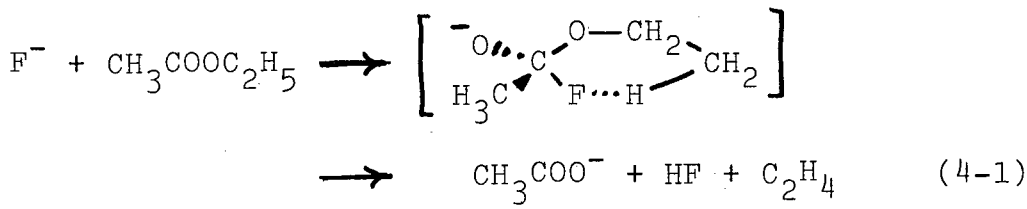

$$\rightarrow \quad CH_3COO^- + HF + C_2H_4 \qquad (4\text{-}1)$$

Very recently Riveros reported the reactions of H^*O^- with various methyl and ethylesters in an effort to determine the importance of $B_{AC}2$, S_N2 and elimination processes.[9] Measurement of the ^{18}O content in product ions was used to establish the importance of these three processes. Riveros concluded that the reaction of H^*O^- with CF_3COOCH_3 goes 24% by a $B_{AC}2$ process and 76% by an S_N2 process while the reaction $H^*O^- + C_6H_5COOCH_3$ goes 92% $B_{AC}2$ and 8% S_N2.

Earlier work by Comisarow showed that the following gas phase reactions occur[11]

$$CD_3O^- + C_6H_5COOCH_3 \longrightarrow C_6H_5COO^- + CD_3OCH_3 \qquad (4\text{-}2)$$

$$CD_3O^- + CF_3COOCH_3 \longrightarrow CF_3COO^- + CD_3OCH_3 \qquad (4\text{-}3)$$

In light of 4-2 and 4-3, an investigation of the reactions of CH_3O^- and $C_2H_5O^-$ with esters in the gas phase by FT-ICR was carried out. Reactions 4-2 and 4-3 were reinvestigated using $CH_3{}^*O^-$ to determine if both $B_{AC}2$ and S_N2 processes were responsible for the formation of the carboxylate anions. Other esters that were included in this study are the alkyl carbonates $(RO)_2CO$ where R is CH_3, CD_3, C_2H_5 or n-C_3H_7. The alkyl carbonates are an ideal system to study because 1) the lack of an acidic proton in the position α to the carbonyl group excludes proton transfer to the nucleophile and 2) the symmetry of the carbonates are helpful in identifying structure-energy relationships.

B. Experimental

i. Instrumental

All work was done on a home built FT-ICR spectrometer which has been described in Chapter 2. Ion ejection techniques were used to confirm reaction pathways and rate constants were measured as described in Chapter 2. Pressure measurements were made with a Varian Model 971-1008 ionization gauge which was calibrated for each gas in the pressure range 10^{-5} to 10^{-4} Torr pressure against an MKS Baratron capacitance manometer. For compounds that have low vapor pressures and are hard to pump, accurate calibrations with the Baratron were not possible. For this reason, the method of Otvos and

Stevenson was used for the calibration of $C_6H_5COOCH_3$ and $(n\text{-}C_3H_7O)_2CO$.[13] Briefly, this method involves calculating the ionization cross-section for a molecule by summing the cross-sections of the atoms which comprise the molecule. The calculated cross-section is then used to determine a calibration factor. For compounds where a calibration factor could be measured accurately as well as calculated, agreement between the two methods was very good. A rate constant of $1.11 \pm .02 \times 10^{-9}$ cm^3/molecule-sec for the reaction $CH_4^+ + CH_4 \longrightarrow CH_5^+ + \cdot CH_3$ was obtained comparing very favorably with an average literature value of 1.11×10^{-9} cm^3/molecule-sec which has been obtained by numerous techniques.[14]

Alkoxide ions in these experiments were generated by electron impact upon the appropriate alkyl nitrite.[15] Thus CD_3ONO gives CD_3O^- and DNO^- in a 3:1 ratio when impacted with .5 - 1.0 eV electrons. CD_3CD_2ONO gives $CD_3CD_2O^-$, DNO^- and CD_2CDO^- under the same conditions. The esters used in these experiments do not display a negative ion ICR signal.

In a typical experiment, nitrite is leaked into the system to a pressure of $\sim 1 \times 10^{-7}$ Torr. An ester is then leaked into the system to achieve a total pressure of about 5×10^{-7} Torr. These pressures are relatively low even by ICR standards because secondary reactions become bothersome at higher pressures. It was desired to study the ratio of reaction products at low conversion percentages in order to deduce mechanistic pathways. Secondary reactions were found

to change product ratios with time, hence both low pressures and low reaction times were needed in these studies. Electron ejection experiments were performed and were found to have no noticeable effect if the filament current was kept low.

ii. Chemicals - Commercial

Whenever possible, chemicals were obtained from commercial sources. Certain chemicals were synthesized by literature methods. Dimethyl carbonate (Aldrich), diethyl carbonate (Eastman), methyl trifluoroacetate (Pierce) and methyl benzoate (Aldrich) were used with no further purification.

iii. Chemicals - Synthesis

Methyl nitrites were synthesized using the appropriately labelled methyl alcohol.[16] CH_3ONO, CD_3ONO and CH_3^*ONO were synthesized.

In a typical preparation, 1.35 g (.042 moles) of MeOH and 2.2 g (.022 moles) of H_2SO_4 in 5 ml H_2O were slowly dripped into a 25 ml, 3 neck flask which contained 3.5 g (.051 moles) of NaONO in 18 ml of H_2O at 0 ^oC. The flask was outfitted with a magnetic stirrer, the addition funnel, N_2 inlet and an outlet tube which lead to a small cold trap which was immersed in an acetone/dry ice slush (-78 ^oC). A pale yellow liquid was collected in the cold trap, distilled on a vacuum line to another trap containing KOH and then finally distilled into a 300 ml glass bulb. The final product is a colorless gas. The glass bulb was stored in the dark to avoid photochemical decomposition.

Ethyl nitrite was prepared in a similar manner starting from CH_3CH_2OH or CD_3CD_2OD (99% D, Stohler Isotopes).

Methanol-^{18}O was prepared by the method of Sawyer[17] in which 15 ml tri-n-butyl orthoformate was hydrolyzed by 1.0 g H_2O^{18} (Norsk Hydro, 99% enriched) under acid conditions to give butyl formate-carbonyl-^{18}O. Reduction of the formate ester with lithium aluminum hydride gave 1.55 g methanol-^{18}O (80% enriched), 85% overall yield based on starting H_2O^{18}.

CD_3OD (99% D) was purchased from Stohler Isotopes.

Deuterated dimethyl carbonate was prepared by the method of Renaud and Leitch.[18] 5 g (.051 moles) of D_3CBr (Stohler Isotopes, 99.5% D) and 7.15 g (.026 moles) of silver carbonate were placed in a thick glass tube. The tube was evacuated on a vacuum line and sealed with a torch. It was placed in an oven at 55 ^{o}C. and occasionally shaken. After 15 days, the tube was opened and the contents distilled yielding 1.1 g (47% yield) of d_6-dimethyl carbonate.

Di-n-propyl carbonate was prepared by the transesterification of dimethyl carbonate.[19] Hence, 40 ml (.53 moles) of n-propanol, .4 g KOH and 10 ml (.123 moles) of dimethyl carbonate were placed in a 100 ml flask and methanol was continuously distilled off. The organic material was washed twice with H_2O, dried over Mg SO_4 and filtered. The crude product was distilled yielding di-n-propyl carbonate.

C. Results

Carboxylate anion is the sole product of the reaction of methoxide and ethoxide with the methyl and ethyl esters used in this study. Proton abstraction by alkoxide was not observed. Table 3 gives the products, per cent of each product at low conversion ratios, rate constants and reaction efficiencies for each reaction done in this study. For all reactions, the neutral products are assumed. Product ratios were determined at low conversion ratios, typically less than 10%, to minimize secondary reactions which lead to product ratios that change with time.

Figure 20 shows the ratio of CD_3OCOO^-/CH_3OCOO^- with time as formed by the reaction

$$CH_3O^- + (CD_3O)_2CO \longrightarrow CH_3OCOO^- + CD_3OCD_3 \qquad (4\text{-}4a)$$

$$\longrightarrow CD_3OCOO^- + CD_3OCH_3 \qquad (4\text{-}4b)$$

The product ratio clearly changes from $\sim$ 2:1 at low reaction times to over 4:1 at longer reaction times. Reaction 4-4 is estimated to be exothermic by about 35 kcal/mole.[20] The products of reaction 4-4, carboxylate anion and neutral, must therefore contain 35 kcal/mole of excess energy between them.

Reaction 4-5 is thermoneutral and is therefore expected to be very slow or nonexistant. However, if CH_3OCOO^- is

$$CH_3OCOO^- + (CD_3O)_2CO \longrightarrow CD_3OCOO^- + CD_3OCOOCH_3 \qquad (4\text{-}5)$$

excited, reaction 4-5 may have an appreciable rate constant.

Buffer gas experiments were performed to determine if

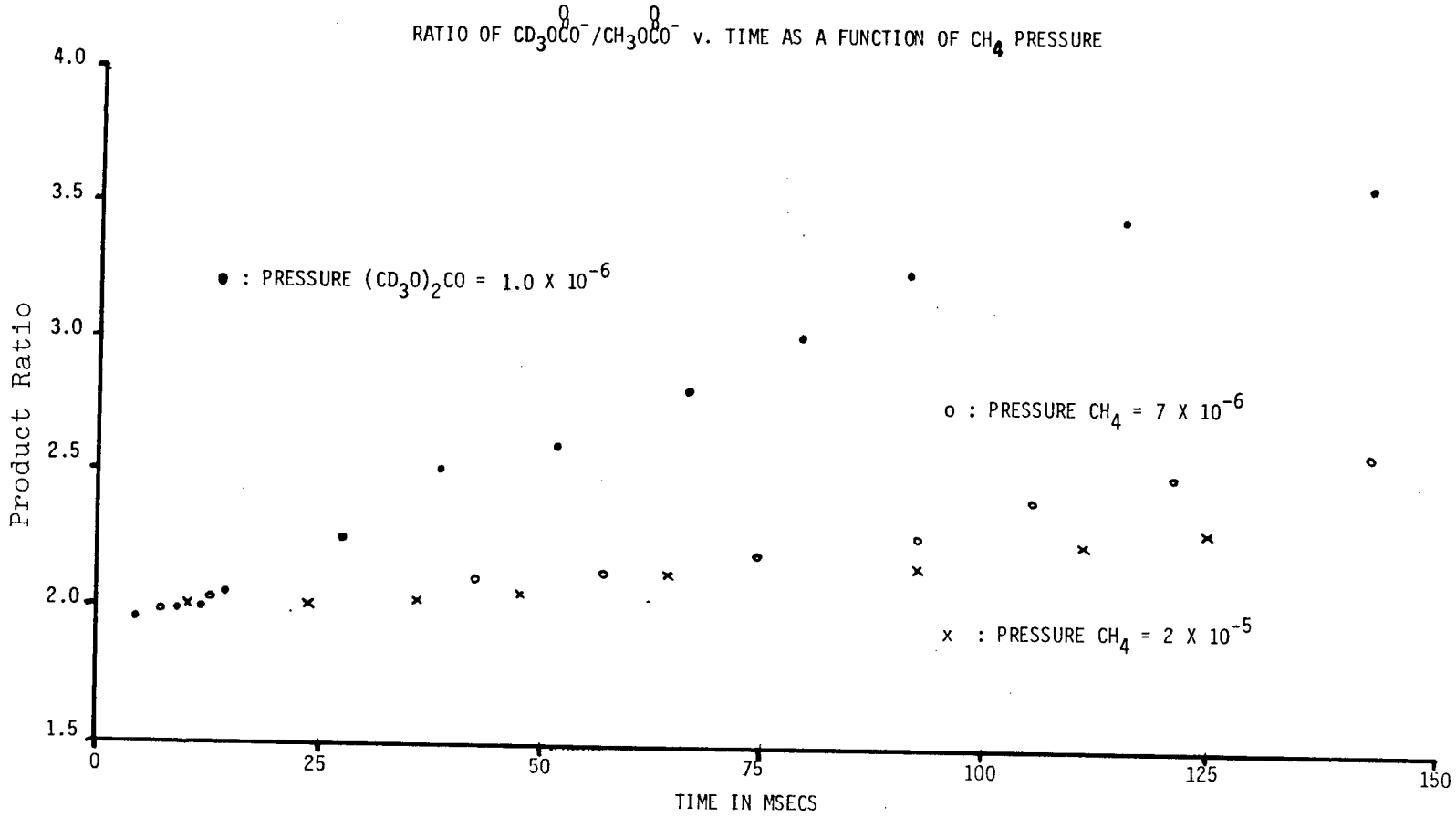

Figure 20 Buffer gas curves for the dimethyl carbonate system.

Table 3 Summary of Reactions Studied

#	ANION	NEUTRAL	PRODUCTS AND %[a]		m/q	K_{exp}[b]	K_{exp}/K_{ADO}[c]	ΔH_{rxn}[d]
1	$CH_3{}^*O^-$	CF_3COOCH_3	$CF_3COO^- + CH_3{}^*OCH_3$	92%	113	8.3	.357	-60
			$CF_3CO{}^*O^- + CH_3OCH_3$	8%	115			
2	$CH_3{}^*O^-$	$C_6H_5COOCH_3$	$C_6H_5COO^- + CH_3{}^*OCH_3$	52%	121	16.9	.732	-54 [11]
			$C_6H_5CO{}^*O^- + CH_3OCH_3$	48%	123			
3	CH_3O^-	$(CD_3O)_2CO$	$CH_3OCOO^- + CD_3OCD_3$	30%	75	5.1	.378	
			$CD_3OCOO^- + CD_3OCH_3$	70%	78			
4	CD_3O^-	$(CH_3O)_2CO$	$CD_3OCOO^- + CH_3OCH_3$	28%	78			
			$CH_3OCOO^- + CD_3OCH_3$	72%	75			
5	$CH_3{}^*O^-$	$(CH_3O)_2CO$	$CH_3OCOO^- + CH_3{}^*OCH_3$	51%	75			
			$CH_3O{}^*COO^- + CH_3OCH_3$	49%	77			
6	$CH_3{}^*O^-$	$(CD_3O)_2CO$	$CH_3{}^*OCOO^- + CD_3OCD_3$	28%	77			
			$CD_3OCOO^- + CD_3{}^*OCH_3$	52%	78			
			$CD_3OCO{}^*O^- + CD_3OCH_3$	20%	80			
7	$CD_3CD_2O^-$	$(CH_3O)_2CO$	$CH_3OCOO^- + C_2D_5OCH_3$ and/or $C_2D_4 + DOCH_3$	84%	75	8.5	.697	
			$C_2D_5OCOO^- + CH_3OCH_3$	16%				

Table 3 Continued

8	CD_3O^-	$(C_2H_5O)_2CO$	$C_2H_5OCOO^-$ + $CD_3OC_2H_5$ and/or CD_3OH + C_2H_4	78%	89	4.12	.23
			CD_3OCOO^- + $C_2H_5OC_2H_5$ and/or C_2H_5OH + C_2H_4	22%	78		
9	$CH_3{}^*O^-$	$(C_2H_5O)_2CO$	$CH_3{}^*OCOO^-$ + neutrals	24%	77		
			$C_2H_5OCO{}^*O^-$ + neutrals	7%	91		
			$C_2H_5OCOO^-$ + neutrals	69%	89		
10	$CD_3CD_2O^-$	$(C_2H_5O)_2CO$	$C_2H_5OCOO^-$ + neutrals	75%	89	4.9	.27
			$C_2D_5OCOO^-$ + neutrals	25%	94		
11	CD_3O^-	$(n\text{-}C_3H_7O)_2CO$	$CH_2{=}CHCH_2O^-$ + neutrals	2%	57	5.45	.26
			$CH_3CH_2CH_2O^-$ + "	44%	59		
			CD_3OCOO^- + "	14%	78		
			$C_3H_7OCOO^-$ + "	40%	103		

Table 3 Continued

12	$CH_3{}^*O^-$	$(n\text{-}C_3H_7O)_2CO$	$CH_2{=}CHCH_2O^-$ + neutrals	2%	57			
			$CH_3CH_2CH_2O^-$ + "	47%	59			
			$CH_3{}^*OCOO^-$ + "	16%	77			
			$C_3H_7OCOO^-$ + "	30%	103			
			$C_3H_7OCO{}^*O^-$ + "	5%	105			
13	$CH_3{}^*O^-$	$CH_3OC_6H_5$	$C_6H_5O^-$ + $CH_3{}^*OCH_3$	100%	93	2.75	.132	-30[d]
14	$CH_3{}^*O^-$	$CH_3CH_2OC_6H_5$	$C_6H_5O^-$ + $CH_3{}^*OCH_2CH_3$	100%	93	12.1	.555	-30[e]
			and/or $CH_3{}^*OH$ + C_2H_4					-14

a % refers to relative amounts of each product at low conversion ratios. b Units for Kexp are 10^{-10} cm^3/molecule-sec. Reactions 3-6 have the same rate constant. Likewise 8,9 and 11,12 are the same. c $Kexp/K_{ADO}$ is the reaction efficiency. K_{ADO} was calculated by the method of M. T. Bowers and T. Su, Theory of Ion Polar Molecule Collisions, in "Interactions Between Ions and Molecules", P. Ausloos, Ed., Plenum Press, New York, 1975. d W. N. Olmstead and J. I. Brauman, J. Amer. Chem. Soc. 99, 4219(1977). e Calculated from heats of formation for $C_2H_5OCH_3$, CH_3OH and C_2H_4 from D. R. Stull, E. F. Westrum, Jr., and G. C. Sinke, "The Chemical Thermodynamics of Organic Compounds", Wiley, New York, 1969. EA for CH_3O and C_6H_5O from K. J. Reed, PhD thesis, Stanford University, 1975.

an excited carboxylate anion is responsible for the product ratio of reaction 4-4 changing with time. From figure 20, it is seen that as the pressure of CH_4 buffer gas is raised, the product ratio approaches a constant value. This shows that the carboxylate anions are becoming thermalized and hence unreactive by collisions with CH_4 which is in a larger number density than the neutral ester. Product ratios for other carbonate reactions in Table 3 were also seen to change with time, presumably due to the same effect.

Experiments with $CH_3{}^*O^-$ were conducted in order to elucidate reaction pathways. $CH_3{}^*O^-$ was formed by the attachment of thermal electrons to $CH_3{}^*ONO$ which was labelled 80% with ^{18}O. HNO^- and CH_3O^-, both m/e=31, are also formed by this process. HNO^- was found to react slowly with esters to yield carboxylate anions. Continuous ejection of CH_3O^- and HNO^- was utilized as described in Chapter 2 to obtain product ratios as a function of time for the methoxide and ethoxide reactions. In this way, methoxide was effectively labelled 100% with ^{18}O and no corrections for unlabelled methoxide were neccessary.

The reaction of $CH_3{}^*O^-$ with methyl trifluoroacetate and methyl benzoate leads to incorporation of $^*O$ in the product ions. Following the arguements of Riveros who studied the reaction of H^*O^- with these two esters, the amount of $^*O$ in the product ions leads to an estimate of the importance of various mechanisms which contribute to the formation of these ions.[9] It will be assumed that reactions 1 and 2 in

Table 3 proceed by two mechanisms: 1) a simple S_N2 process where the methoxide attacks the alkyl group, that is attack is at the methyl group and 2) attack of methoxide is at the carbonyl carbon to form a tetrahedral intermediate which can rearrange to give products; that is, a $B_{AC}2$ type process. If the assumption is made that the methoxy groups in the tetrahedral intermediate are equivalent, the relative importance of S_N2 and $B_{AC}2$ type processes can be estimated from the $^*O$ content in the products. Table 4 gives the $CH_3{}^*O^-$ results along with the H^*O^- results of Riveros for comparison. It is seen that the reactions of $CH_3{}^*O^-$ and H^*O^- with methyl trifluoroacetate and methyl benzoate are similar.

Table 4 Contribution of $B_{AC}2$ and S_N2 to Selected Gas Phase Reactions

Reactants	$B_{AC}2$	S_N2
$H^*O^- + CF_3COOCH_3$	24%	76%
$CH_3{}^*O^- + CF_3COOCH_3$	16%	84%
$H^*O^- + C_6H_5COOCH_3$	92%	8%
$CH_3{}^*O^- + C_6H_5COOCH_3$	96%	4%

The reaction of methoxide and ethoxide with methyl and ethyl carbonate leads to the exclusive formation of carboxylate anions. However, the reaction of methoxide with n-propyl carbonate yields propoxide as well as carboxylates. Figures 21 and 22 give the temporal ion intensities for reactions 11 and 12 of Table 3 showing that propoxide is an initial product which reacts further with n-propyl carbonate. An ion at m/e = 57 is also formed in small amounts which appears to be unreactive with n-propyl carbonate.

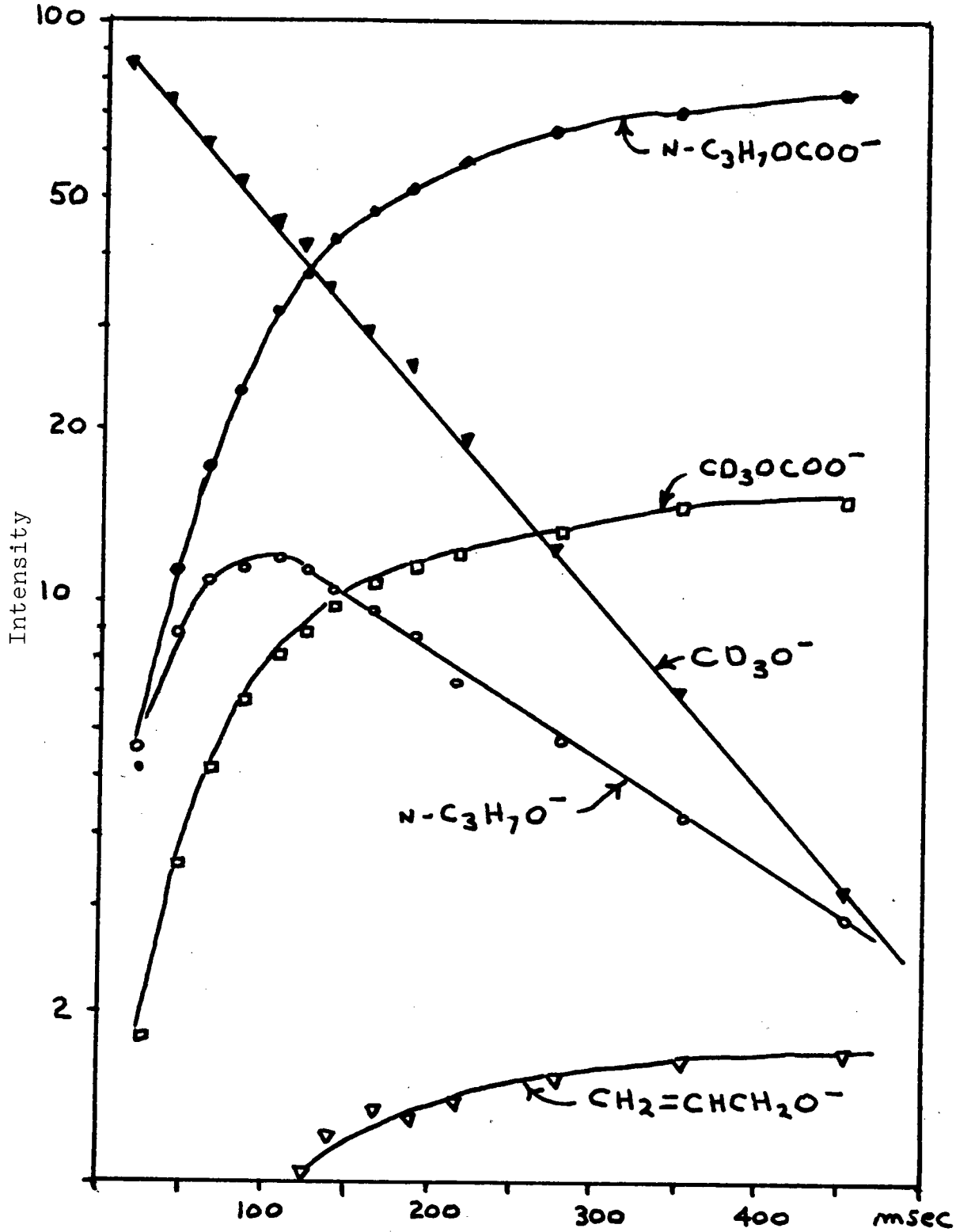

Figure 21 Time plot for CD_3O^- + $(n\text{-}C_3H_7O)_2CO$ → products.

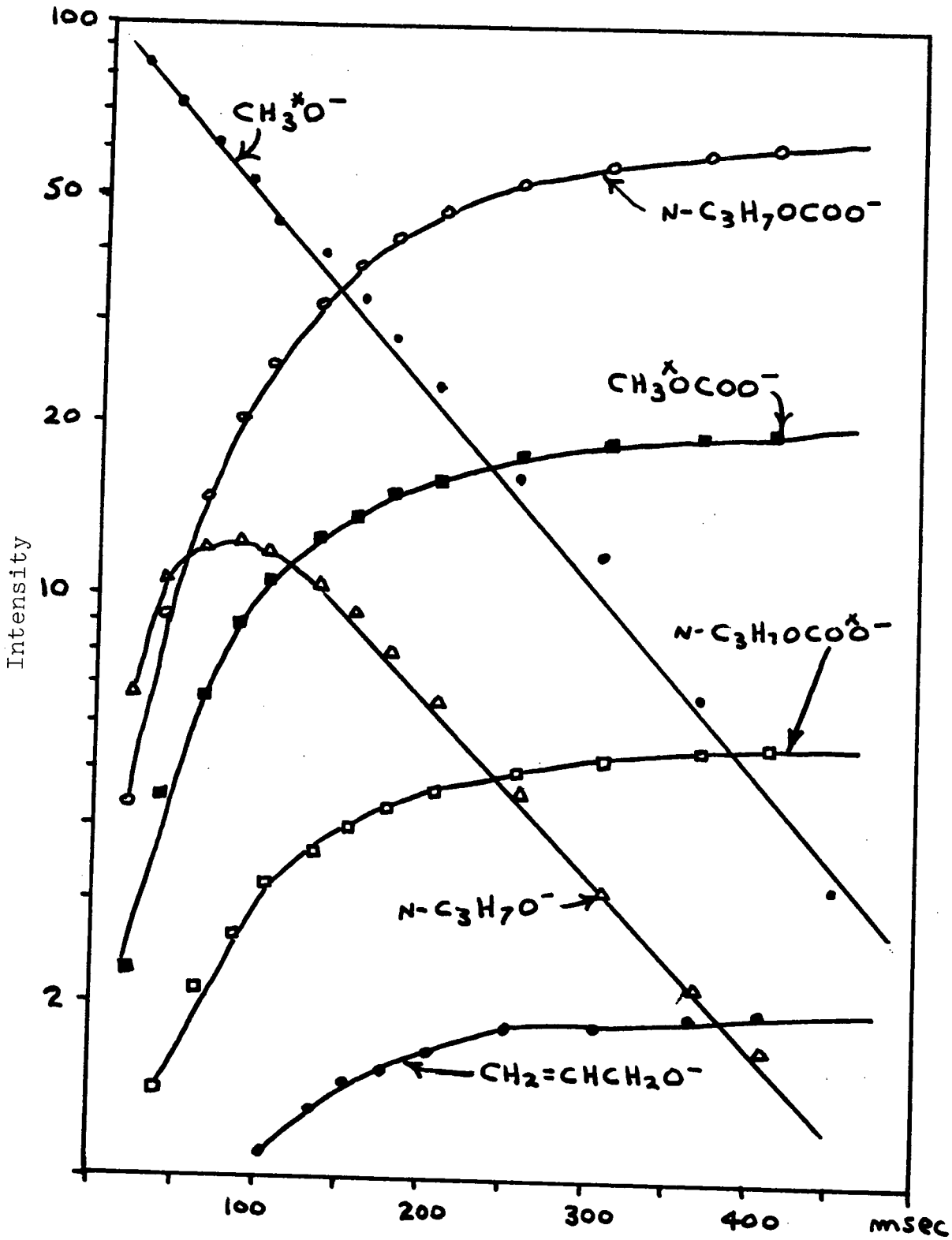

Figure 22 Time plot for $CH_3{}^*O^-$ + $(n\text{-}C_3H_7O)_2CO$ → products.

It has been reported that the reactions of ethyl esters with negative ions have a higher reaction efficiency than methyl esters due to the presence of β hydrogens which open up an elimination channel.[7,8] Since experiments with $CH_3{}^*O^-$ and H^*O^- show that both S_N2 or elimination and $B_{AC}2$ type processes lead to the formation of carboxylate anions, it is desirable to know how much β hydrogens can speed up product formation.

Control experiments with anisole and phenetole were performed to determine the influence of β hydrogens on reaction efficiency. These compounds are expected to form products only by S_N2 and/or elimination processes. The reaction of $CH_3{}^*O^-$ with anisole and phenetole leads only to phenoxide. No $^*O$ is seen in the product ions showing that as expected, only S_N2 and/or elimination reactions are occurring. From Table 3, it is seen that phenetole reacts with methoxide approximately four times as fast as anisole. Thus, the presence of β hydrogens can increase the reaction efficiency due to elimination by up to a factor of four in some cases.

D. Discussion of Results

The results in Table 3 show that methyl esters react predominantly by a $B_{AC}2$ type process as judged by the amount of $^*O$ incorporation in the product ions. Ethyl esters have less $^*O$ showing the increased importance of elimination. A $B_{AC}2$ type process is in accord with theoretical calculations by Tomasi who showed that tetrahedral intermediates of carbonyl systems are expected to lie on an energy minima.[21]

For the reaction,

$$HO^- + H_2NCHO \longrightarrow NH_3 + HCOO^- \qquad (4\text{-}6)$$

the intermediate from addition of HO^- to the carbonyl group was calculated to be stable compared to reagents by 104 kcal/mole. Also, tetrahedral intermediates have been detected in the gas phase by ICR lending credence to the suggestion that reactions 1-12 in Table 3 proceed at least partially via a $B_{AC}2$ or tetrahedral process.

As mentioned previously, simple calculations show the relative importance of $B_{AC}2$ and S_N2 type processes for CF_3COOCH_3 and $C_6H_5COOCH_3$. However, the validity of the assumption concerning an energy randomized tetrahedral intermediate can not be ascertained at this juncture in time for these two esters. The reaction of methoxide with dimethyl carbonate should yield information concerning this assumption as a symmetrical intermediate may be formed.

Reactions 3-6 of Table 3 utilize various labels to study the dimethyl carbonate/methoxide system. Various internal consistencies are noted. Thus, reactions 3,4 and 6 which utilize deuterium labelling each show that there is a 70:30 ratio of H/D or D/H in the product ions. Reactions 5 and 6 use ^{18}O labelling and each gives the same amount of ^{18}O in the product ions, about 50%. These internal consistencies are important in that they preclude the influence of isotope effects and show that the measurements are not influenced by experimental techniques or instrumental artifacts, problems

that must be reconciled when dealing with new instrumentation or methods.

Reaction 6 is particularly informative concerning the mechanism of reaction. Scheme I outlines the products of reaction 6 that would be expected for an S_N2 process only while Scheme II gives the products for a $B_{AC}2$ type process which proceeds through an energy randomized tetrahedral intermediate.

Scheme I

$$CH_3{}^*O^- + CD_3OCOOCD_3 \longrightarrow [CH_3{}^*O\cdots CD_3\cdots OCOOCD_3]^-$$

$$\downarrow$$

$$CH_3{}^*OCD_3 + CD_3OCOO^- \quad 100\%$$

(m/e=78)

Scheme II

$$CH_3{}^*O^- + CD_3OCOOCD_3 \longrightarrow \left[CH_3{}^*O\overset{O^-}{\underset{O:}{C}}OCD_3\right]$$

$$\downarrow$$

$$CH_3{}^*OCD_3 + CD_3OCOO^- \quad 33\%$$

(m/e=78)

$$CH_3OCD_3 + CD_3OCO{}^*O^- \quad 33\%$$

(m/e=80)

$$CD_3OCD_3 + CH_3{}^*OCOO^- \quad 33\%$$

(m/e=77)

Figure 23 is a spectrum of the products of reaction 6

taken at low reaction time. No product at m/e = 75, corresponding to CH_3OCOO^-, was seen showing that there is no scrambling of methyl groups occurring in the intermediate of Scheme II. Scheme I produces mass 78 only while Scheme II produces 77,78 and 80 in equal amounts. Thus, if reaction 6 proceeds only via processes depicted in Schemes I and II, products at m/e = 77 and 80 should appear in equal amounts. However, inspection of the results shows this not to be the case, m/e = 77 is formed in 28% yield while m/e = 80 is formed in only 20% yield.

Implications of these results are: 1) the formation of a true tetrahedral intermediate is not neccessary for reaction to occur, or 2) another mechanism is in effect. No other suitable mechanism can be given that will fit the products observed. However, reactions of esters which proceed from nonequilabrated positions have been reported by Riveros lending credence to the former implication.[6]

The reaction of $CH_3{}^*O^-$ with ethyl and n-propyl carbonates is characterized by the diminishing abundance of $^*O$ in the product ions. Total ^{18}O incorporation in the products is seen to be 31% and 21% for the ethyl and n-propyl carbonates respectively. However, the reaction efficiency is not seen to increase over the methyl carbonate system showing that attack of the nucleophile at the carbonyl carbon is still important. An elimination channel is now open with the presence of β hydrogens. Elimination could conceivably occur by direct attack of the nucleophile on the alkyl group or

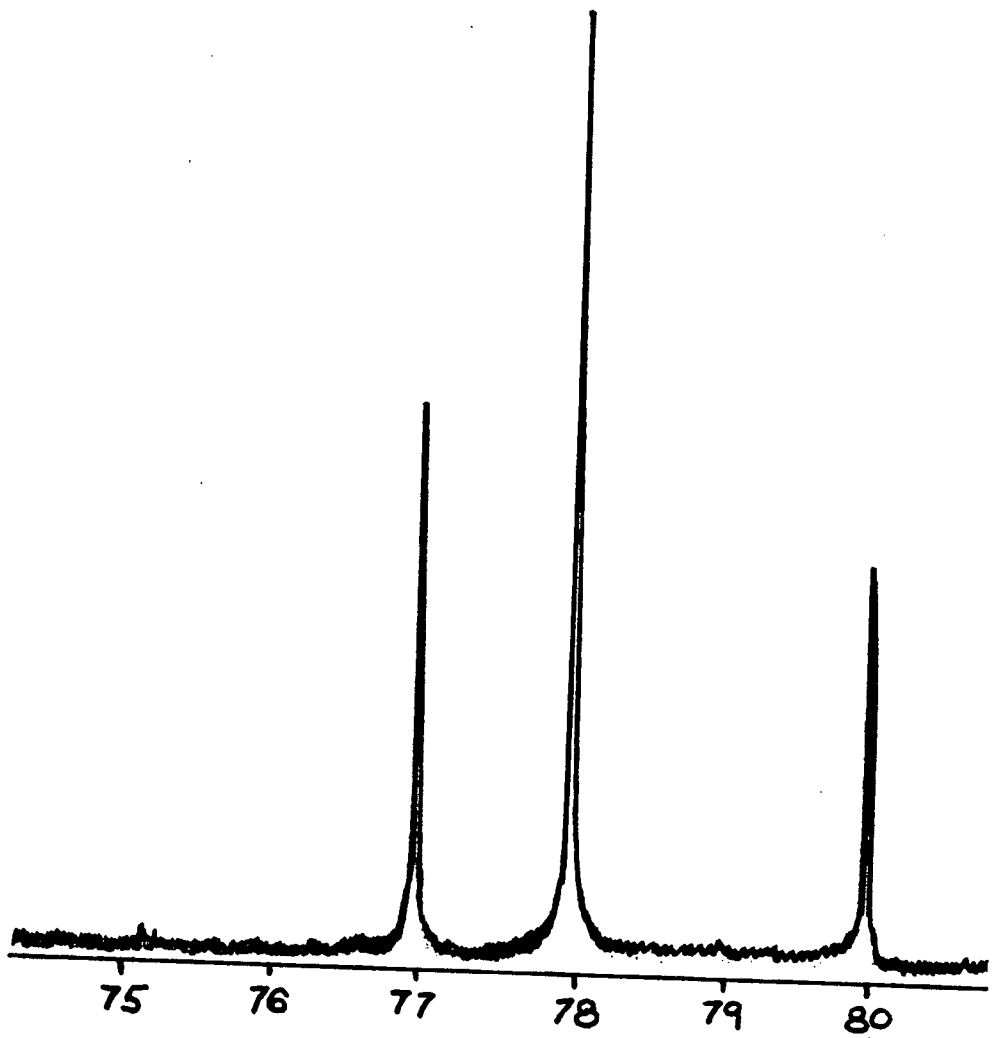

Figure 23 Products of $CH_3{}^*O^-$ + $(CD_3O)_2CO$ at low reaction time.

through an intermediate such as,

Scheme III

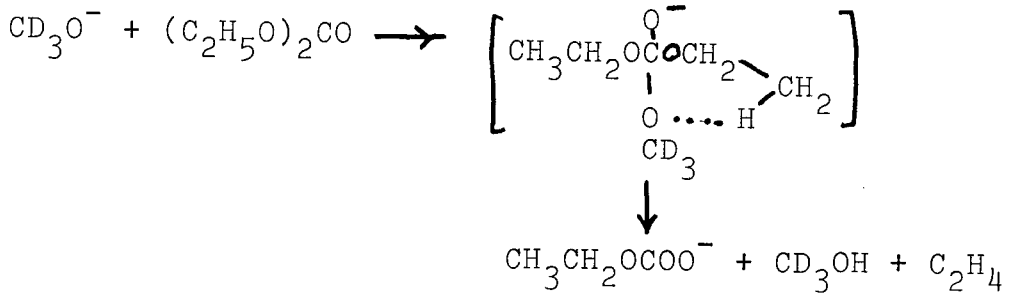

Presumably, similar processes can occur in the propyl carbonate system.

Formation of an alkoxide is first seen in the reaction of methoxide with n-propyl carbonate. Propoxide could be formed as follows

Scheme IV

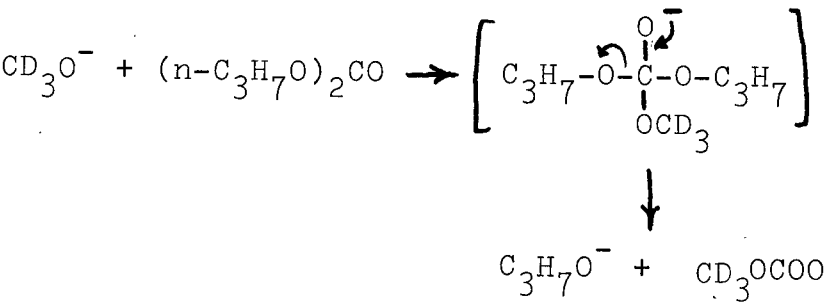

Carboxylates could be formed by the rearrangement of the intermediate in Scheme IV or by a process similar to that in Scheme III, also by direct S_N2 attack. The identity of the product at m/e = 57 has been assigned to $CH_2{=}CHCH_2O^-$ although this has not been substantiated by experiment. Deuterium labelling of the propyl group could help to identify this ion.

The reaction of ethoxide with methyl and ethyl carbonate leads to carboxylate anions. These reactions appear to be

very similar to the methoxide reactions and presumably no new mechanisms need to be introduced.

The process by which an intermediate such as that depicted in Scheme II rearranges to products is open to speculation. The simplest explanation involves a four-center mechanism such as

Scheme V

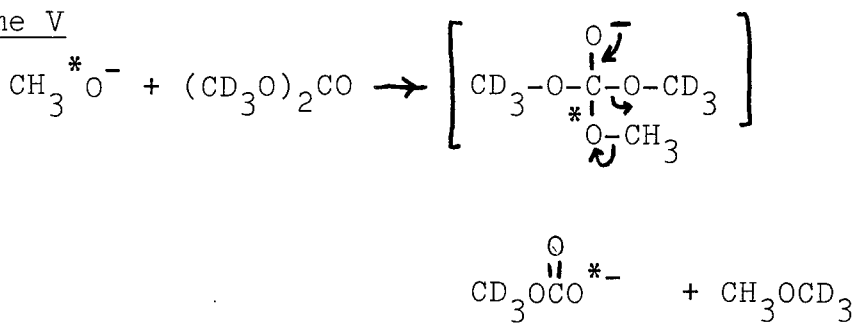

Four center mechanisms have also been postulated for the gas phase reactions of methoxide with fluoroalkanes,[23]

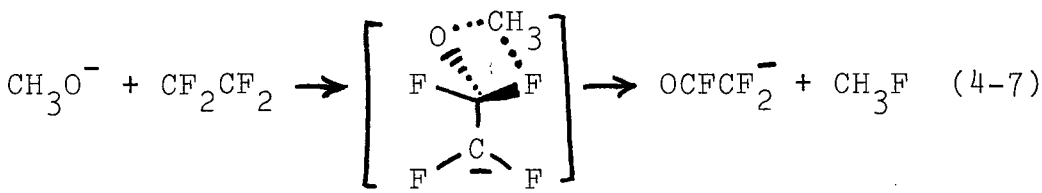

(4-7)

Beauchamp has studied the reactions of various alkoxides with fluoroalkanes and arrived at conclusions similar to those presented here; direct elimination of F^- or OR^- anions does not occur. Rather, rearrangement occurs to eliminate an energetically favorable neutral such as HF, CH_3F etc.. For esters used in this study (except $(n\text{-}PrO)_2CO$), the same conclusions hold. ROR' is eliminated from an intermediate rather than RO^-.

Riveros has studied the reaction of $H^{*}O^-$ with some of

the esters used in this study and also arrived at the same conclusion that direct elimination of RO^- is not a favored pathway for some esters.[9] This does become important for alkyl pivalates however,

$$CD_3O^- + (CH_3)_3CCOOCH_3 \xrightarrow{K_{BAC^2}} CH_3O^- + (CH_3)_3CCOOCD_3$$
$$\xrightarrow{K_{S_N2}} (CH_3)_3CCOO^- + CD_3OCH_3 \quad (4\text{-}8)$$

where $K_{B_{AC}2}/K_{S_N2} = 1.5$.

This work has shown that the gas phase reactions of negative ions with esters contains very rich chemistry. Further studies should include nucleophiles containing S and N to see if new reaction paths are opened. Also, varying the alkyl group on the ester will lead to a better understanding of the forces that determine how much of the reaction goes by a particular mechanism. A reaction that has been studied only briefly that offers a glimpse of the potential for study and interpretation in this area of gas phase chemistry is

$$DNO^- + (RO)_2CO \longrightarrow ROCOOCH_2^- + ???$$
$$ROCOO^- + ??? \quad (4\text{-}9)$$

where R is CH_3, CH_3CH_2 or $n\text{-}C_3H_7$.

REFERENCES AND NOTES

1. "The Chemistry of the Carbonyl Group", S. Patai, Ed., Interscience, New York, 1966.

2. Polanyi and Szabo, Trans. Faraday Soc. 30, 508(1934).

3. M. L. Bender, J. Am. Chem. Soc., 73, 1626(1951).

4. J. McMurry in "Organic Reactions, Vol. 24", W. G. Dauben, Ed., New York, 1976.

5. L. K. Blair, P. C. Isolani and J. M. Riveros, J. Amer. Chem. Soc. 95, 1057(1973).

6. P. W. Tiedman and J. M. Riveros, J. Am. Chem. Soc. 96, 185(1974).

7. J. F. G. Faigle, P. C. Isolani and J. M. Riveros, J. Amer. Chem. Soc. 98, 2049(1976).

8. S. M. Jose and J. M. Riveros, Nouveau.J. Chim 1, 113(1977).

9. K. Takashima and J. M. Riveros, J. Amer. Chem. Soc. 100, 6128(1978).

10. O. I. Asubiojo, L.K. Blair and J. I. Brauman, J. Amer. Chem. Soc. 97, 6685(1975).

11. M. B. Comisarow, Can. J. Chem. 55, 171(1977).

12. W. N. Olmstead and J. I. Brauman, J. Amer. Chem. Soc. 99, 4219(1977).

13. J. W. Otvos and D. P. Stevenson, J. Am. Chem. Soc. 78, 546(1956).

14. W. T. Huntress, J. B. Laudenslager and R. F. Pinizzotto, Int. J. Mass Spectrom. Ion Phys. 13, 331(1974).

15. K. Jager and A. Heinglein, Z. Naturforsch. A., 22,700(1967).

16. D. F. Hunt, G. C. Stafford, F. W. Crow and J. W. Russel, Anal. Chem. 48, 2098(1976).

17. C. B. Sawyer, J. Org. Chem. 37, 4225(1972).

18. R.Renaud and L. C. Leitch, Can. J. Chem. 34, 181(1956).

19. L. S. Bondar, P. P. Rodionov, V. I. Pauskii, V. A. Masten and R. A. Okunev, Izv. Akad. Nauk SSSR, Serthim 1972, 308. Chem. Abstracts 77-19122.

20. ΔHrxn was determined from a Born cycle. E.A. for $CH_3O\cdot$ is 36.65 kcal/mole from K. J. Reed, Ph.D. Thesis Stanford University, 1975, p. 273. E.A. for $CH_3OCOO\cdot$ was estimated to be 79.5 kcal/mole. Bond energies used were $D(CH_3COO—CH_3)$=88 kcal/mole and $D(H_3C—OCH_3)$=80 kcal/mole from J. A. Kerr, Chem. Rev. 66, 465(1966).

21. G. Alagona, E. Scrocco and J. Tomasi, J. Amer. Chem. Soc. 97, 6976(1975).

22. J. H. Bowie and B. D. Williams, Aust. J. Chem. 27, 1923 (1974).

23. S. A. Sullivan and J. L. Beauchamp, J. Amer. Chem. Soc. 99, 5017(1977).